

POEMMA's target of opportunity sensitivity to cosmic neutrino transient sources

Tonia M. Venters

Astrophysics Science Division, NASA Goddard Space Flight Center, Greenbelt, MD 20771, USA

Mary Hall Reno

Department of Physics and Astronomy, University of Iowa, Iowa City, IA 52242, USA

John F. Krizmanic

*CRESST/NASA Goddard Space Flight Center, Greenbelt, MD 20771, USA
University of Maryland, Baltimore County, Baltimore, MD 21250, USA*

Luis A. Anchordoqui

*Department of Physics, Graduate Center, City University of New York (CUNY), NY 10016, USA
Department of Physics and Astronomy, Lehman College (CUNY), NY 10468, USA
Department of Astrophysics, American Museum of Natural History, NY 10024, USA*

Claire Guépin

Sorbonne Université, CNRS, UMR 7095, Institut d'Astrophysique de Paris, 98 bis bd Arago, 75014 Paris, France

Angela V. Olinto

*Department of Astronomy & Astrophysics, KICP, EFI,
The University of Chicago, Chicago, IL 60637, USA
(Dated: November 15, 2021)*

We calculate the sensitivity of space-based cosmic neutrino detection from transient sources in the context of the Probe Of Extreme Multi-Messenger Astrophysics (POEMMA) mission using Target-of-Opportunity (ToO) observations. POEMMA uses two spacecraft each with a large Schmidt telescope to simultaneously view the optical signals generated by extensive air showers (EASs). POEMMA is designed for both ultrahigh-energy cosmic ray and very-high-energy neutrino measurements. POEMMA has significant neutrino sensitivity starting in the 10 PeV decade via measurements of Cherenkov signals from upward-moving EASs initiated by tau neutrinos interacting in the Earth. For ToO observations, POEMMA uses the ability to quickly repoint (90° in 500 seconds) each of the two spacecraft to the direction of the transient source. POEMMA EAS measurements are performed during astronomical night, leading to different observational constraints for short- and long-duration bursts. For short-bursts of order 10^3 s, POEMMA will increase the sensitivity of existing experiments (e.g., IceCube and the Pierre Auger Observatory) by up to two orders of magnitude. For long-duration bursts on the scale of 10^{5-6} s, the full celestial sky is available and the average neutrino sensitivity will be increased by up to a factor of 50, reaching the desired level to probe model predictions of transient neutrino sources (e.g., of blazar flares as well as both black hole-black hole and neutron star-neutron star mergers). POEMMA's neutrino sensitivity to various models of transient neutrino sources are detailed. Altogether, our results demonstrate better sensitivity to ToO neutrino sources from the space-based POEMMA experiment compared to current ground-based experiments, and more importantly, demonstrate unique full-sky coverage for ToO neutrino sources.

I. INTRODUCTION

Astrophysical transients are now a staple of multi-wavelength observations of electromagnetic signals by ground-based and space-based telescopes. In

the last few years, multi-messenger astronomy has blossomed with coincident observations of photons and gravitational waves or high-energy neutrinos. In 2017, LIGO reported the groundbreaking observation of gravitational waves from a neutron star-

neutron star merger [1] coincident with a number of electromagnetic signals [2]. In 2018, the correlation of a neutrino event in IceCube with multi-wavelength observations of a blazar [3] heralded the beginning of multi-messenger programs using high-energy neutrinos. The next decade should witness the simultaneous observation of three astronomical messengers: photons, neutrinos, and gravitational waves, from the same astrophysical transients.

Here we derive the unique contributions to the multi-messenger studies of transient phenomena of a space-based mission designed to observe neutrinos above 10 PeV. Below about PeV energies, ground-based neutrino detectors [4–11] have the benefit of full sky coverage, but above such a critical energy large areas of the sky become inaccessible to a given ground-based observatory because the Earth attenuates higher energy neutrinos. Space-based neutrino detectors, while typically restricted in field-of-view, can be re-pointed to respond to astrophysical source alerts throughout the full sky. For long transients, space-based instruments have the advantage of full sky coverage given the orbital motion and the precession of the orbit. For shorter transients, fast re-positioning provides access to all sources that produce signals in the dark sky.

Astrophysical neutrino transient sources come from a wide range of phenomena [12, 13]. Gamma-ray burst (GRB) emission is a textbook example [14–16]. In tidal disruption events (TDEs), supermassive black holes (SMBHs) pull in stellar material that interacts with thermal and non-thermal photons to produce neutrinos [17, 18]. Blazar flares, dominant sources of extragalactic gamma rays, may be important neutrino sources [3, 19]. Neutrino fluence predictions from black hole-black hole (BH-BH) [20] and neutron star-neutron star (NS-NS) [21] mergers may tie sources of gravitational waves and electromagnetic signals to neutrino signals. Neutrinos, not gamma rays, may be the primary signal of cosmic-ray acceleration in white dwarf-white dwarf (WD-WD) [22] mergers. The spin-down of newly-born pulsars ultimately produces cosmic rays that may interact with the hadronic environment to produce neutrinos [23].

Neutrino and antineutrino production in these transient astrophysical sources is dominated by pion production for a large range of energies. At the energies of interest here, the neutrino- and antineutrino-nucleon cross sections are effectively equal [24], so we do not distinguish between neutrinos and antineutrinos. To a first approximation, charged pion decay gives two muon neutrinos for each electron neutrino [25]. The nearly maximal mixing of muon neutrinos and tau neutrinos in the Pontecorvo-Maki-Nakagawa-Sakata matrix of neutrino flavor mix-

ing [26] results in approximately equal electron neutrino, muon neutrino, and tau neutrino fluxes at the Earth [27]. Upward-going tau neutrinos that interact in the Earth can produce taus that decay in the atmosphere. They provide a unique signal for satellite-based or balloon-borne instruments [28–38], and Earth-based instruments like the Pierre Auger Observatory [39–43] or other surface arrays [44–48].

For large path lengths through the Earth, the high-energy neutrino flux is attenuated. However, Earth-skimming neutrinos that emerge with relatively small elevation angles can produce air shower signals. Tau neutrinos have the added feature that the tau neutrino flux attenuation can be somewhat mitigated by regeneration, since the secondary tau could decay and produce a tau neutrino albeit at a lower energy [49–53].

The Probe Of Extreme Multi-Messenger Astrophysics (POEMMA) [34] is a space-based mission described in the NASA Astrophysics Probe study report [54]. POEMMA is optimized for the measurement of extensive air showers (EASs) from ultrahigh-energy cosmic rays (UHECRs) using the stereo air fluorescence technique, and from neutrino induced upward-going EASs via optical Cherenkov detection. POEMMA satellites in neutrino mode (pointing near the limb of the Earth) will have the ability to follow up Target-of-Opportunity (ToO) alerts with quick re-pointing of the telescopes to the transient source direction. POEMMA operates during astronomical night in order to measure the near-UV air fluorescence and 300 – 900 nm optical Cherenkov EAS signals.

The POEMMA satellite-based detectors are planned to orbit in tandem with a separation scale of the order of 100 km at an altitude of $h = 525$ km, and with an orbital period of $T_s = 95$ min. The orbital plane is oriented at an angle of $\xi_i = 28.5^\circ$ relative to the Earth’s polar axis, and the precession period is $T_p = 54.3$ days. For neutrino bursts with short time scales ($\sim 10^3$ s), the orbit of the satellites around the Earth allows for nearly full sky coverage, assuming adequate target visibility. The added precession of the orbital plane of the satellites over a few month time span ensures that long duration neutrino bursts ($\sim 10^5 - 10^6$ s) will come into view regardless of celestial position [55].

The focal plane of each POEMMA telescope contains an edge sector that is optimized for optical Cherenkov detection, with a field of view of $\sim 30^\circ \times 9^\circ$ for neutrino observations. In diffuse flux neutrino mode, the POEMMA instruments will be tilted to cover a viewing area extending from 7° below the horizon to 2° above it, equivalent to covering tau trajectories emerging from the Earth with elevation angles $\beta_{tr} \lesssim 20^\circ$ [55, 56]. To follow a ToO flar-

ing neutrino source, the POEMMA telescopes can slew to larger angles below the horizon, keeping the source direction well within the $\sim 30^\circ \times 9^\circ$ neutrino field of view, even after accounting for the few degree smearing due to the Cherenkov emission angle. POEMMA's capability to slew its pointing, on the order of 500 s to shift 90° , makes this NASA mission responsive to alerts of flares in neutrinos and other astrophysical messengers.

ToO observations will bring the two POEMMA spacecraft to a separation of ~ 50 km in order to put both telescopes into the Cherenkov light pool. The nearly simultaneous measurement of the Cherenkov signal with both telescopes with a time spread of ~ 20 ns allows for a lower energy threshold for POEMMA by using coincidence timing to reduce the effects due to the air glow background in the 300 – 900 nm Cherenkov signal band.

In this paper, we evaluate the sensitivity of POEMMA to transient sources for both long and short neutrino bursts. The layout is as follows. We begin in Sec. II with a calculation of the effective area, the exposure, and the sensitivity of POEMMA to neutrino fluxes. In Sec. III, we describe our evaluation of the number of events from a flaring neutrino source, and we determine the maximum luminosity distance at which POEMMA will detect one neutrino from the given source. We conclude in Sec. IV. Some details for the effective area evaluation are included in Appendix A. Appendix B shows the relation between isotropic equivalent source characteristics and the fluence observed at a source luminosity distance.

II. POEMMA'S EFFECTIVE AREA, EXPOSURE, AND SENSITIVITY

The effective area evaluation begins with the geometrical configuration of an instrument at $h = 525$ km above the Earth. For measurements of the diffuse flux, more than $4,000 \text{ km}^2 \text{ sr}$ of geometric aperture is accessible to POEMMA [56]. For point sources, the evaluation of the effective area depends on the elevation angle β_{tr} of the tau trajectory and the elevation angle of the line of sight to the detectors from the point on the Earth at which the tau emerges (the length of the line of sight is given by v). The decay length of the tau along the line of sight is s . Details of the geometry are given in Ref. [56] and described here in Appendix A.

The ToO sensitivity at a given time depends on the area A_{Ch} subtended on the ground by the Cherenkov cone. For a shower produced along the tau trajectory emerging at angle β_{tr} from a tau decay at altitude a , with a pathlength before decay

$s(\beta_{\text{tr}}, a)$, we approximate

$$A_{\text{Ch}}(s) \simeq \pi(v - s)^2 \times (\theta_{\text{Ch}}^{\text{eff}})^2, \quad (1)$$

where we take $\beta_v(t) \simeq \beta_{\text{tr}}(t)$ and $\theta_{\text{Ch}}^{\text{eff}}$ is the effective Cherenkov angle that takes into account the altitude dependence and a broadening due to an increase in instrument acceptance for more intense signals (see App. A). The effective Cherenkov angle depends on β_{tr} , the decay altitude a , and the shower energy $E_{\text{shr}} \simeq 0.5E_\tau$. The effective area for ν_τ detection is

$$A(\beta_{\text{tr}}(t), E_\nu) \simeq \int dP_{\text{obs}}(E_\nu, \beta_{\text{tr}}, s) A_{\text{Ch}}(s), \quad (2)$$

where the differential probability to observe the τ shower is

$$dP_{\text{obs}}(E_\nu, \beta_{\text{tr}}, s) = ds P_{\text{exit}}(E_\nu, \beta_{\text{tr}}) p_{\text{dec}}(s) \times P_{\text{det}}(E_\nu, \beta_{\text{tr}}, s), \quad (3)$$

and where P_{exit} is the exit probability, p_{dec} is the decay distribution, and P_{det} is the detection probability.

The exit probability $P_{\text{exit}}(E_\nu, \beta_{\text{tr}})$ depends on the tau neutrino cross section in Earth, the tau energy distribution from the interaction, and tau energy loss and decay as it transits through the Earth. Throughout this paper we evaluate the neutrino-nucleon cross section using the nCTEQ15 parton distribution functions [57] and adopt the Abramowicz-Levin-Levy-Maor (ALLM) parameterization of the proton structure function [58, 59] for photonuclear energy loss, as discussed in more detail in Ref. [56]. The tau exit probabilities are shown in Fig. 12 of Appendix A. For angles to $\sim 18^\circ$ below the horizon, the emergent tau trajectory elevation angles are $\beta_{\text{tr}} \leq 35^\circ$. For $\beta_{\text{tr}} = 35^\circ$, neutrino attenuation in the Earth gives the probability for a tau neutrino to produce an exiting tau to be less than 10^{-5} for the energies of interest. Thus, our evaluation of Eq. (2) for $\beta_{\text{tr}} \leq 35^\circ$ is a good approximation to the full angular range.

The differential decay distribution is

$$p_{\text{dec}}(s) ds = B_{\text{shr}} \exp(-s/\gamma c\tau_\tau) \frac{ds}{\gamma c\tau_\tau}, \quad (4)$$

where the tau branching fraction to showers is $B_{\text{shr}} = 0.826$ (excluding the muon channel with branching fraction $\sim 17.4\%$).

Finally, the detection probability is approximated by

$$P_{\text{det}} \simeq H[N_{\text{PE}} - N_{\text{PE}}^{\text{min}}], \quad (5)$$

in terms of the Heaviside function $H(x)$:

$$H(x) = \begin{cases} 0 & \text{if } x < 0 \\ 1 & \text{if } x \geq 0 \end{cases}.$$

The number of photo-electrons (PE), N_{PE} , is determined from a model of the photon density from the tau induced air showers assuming $E_{\text{shr}} = 0.5E_{\tau}$, as a function of shower energy, altitude of decay and β_{tr} , multiplied by the collecting area of each detector and the quantum efficiency for photo-detection. The N_{PE} calculation uses the Cherenkov intensity delivered to the POEMMA instruments using the same model of the atmospheric attenuation of the Cherenkov signal than in Ref. [56]. We use an optical collection area of 2.5 m^2 and a quantum efficiency of 0.2, and we set the threshold for detection of $N_{\text{PE}}^{\text{min}} = 10$ for POEMMA. Reference [56] outlines the considerations in setting this threshold. Figures 13 and 14 in Appendix A show the effective Cherenkov angle and photon density as a function of elevation angle and altitude of tau decay for $\beta_{\text{tr}} \leq 40^\circ$.

In calculating the detection probability, a more detailed Monte Carlo simulation was used in Ref. [56] to account for $\beta_{\nu} \neq \beta_{\text{tr}}$ and to impose the requirement that tau decay within an observation window that depends on the emergence angle and altitude of decay in order to produce detectable air showers. The simplification in Eq. (5) is a very good approximation to the more detailed evaluation of the detection probability for the diffuse flux [56], so we use it here for the ToO sensitivity.

To determine the sensitivity for a burst, the time averaged effective area is required:

$$\langle A(E_{\nu}, \theta, \phi) \rangle_{T_0} = \frac{1}{T_0} \int_{t_0}^{t_0+T_0} dt A(\beta_{\text{tr}}(t), E_{\nu}, \theta, \phi), \quad (6)$$

for a source celestial position location labeled with θ and ϕ . For long-duration sources, where the source emits neutrinos for a much longer time than the orbital period of POEMMA ($T_s = 95 \text{ min} = 5.7 \times 10^3 \text{ s}$), we use the orbit averaged value, so $t_0 = 0$ and $T_0 = T_s$. For short bursts, we find the average effective area for $T_0 = T_{\text{burst}}$. We use $T_{\text{burst}} = 10^3 \text{ s}$ as a representative short burst time in the results shown below.

For sources that dip just below the horizon as the POEMMA satellites orbit, the effective area is optimal. Some sources, for a specific satellite orbit, are not observable. The upper panel of Fig. 1 shows the fractional time exposure in equatorial celestial coordinates for points in the sky coverage for a given orbital position integrated over one orbit, neglecting the impact of the Sun and the Moon on the observation.

In the lower panel of Fig. 1 we show the effect of the Sun and Moon combined for the fraction f_t that reduces $\langle A \rangle$. This fraction is source location dependent. To a first approximation, over long

periods, the Sun eliminates half of the observing time. The bright Moon further reduces the observing time, again dependent on source location by a factor of $0.63 - 0.87$. The range of values is between $0.2 \lesssim f_t \lesssim 0.4$.

For the neutrino sensitivity curves of long duration bursts, we use the approximate relation

$$\text{Sensitivity} = \frac{2.44}{\ln(10)} \times \frac{N_{\nu} E_{\nu}}{f_t \langle A(E_{\nu}) \rangle_{T_0}}, \quad (7)$$

with $T_0 = T_s$. We have taken a 90% unified confidence level [60] over a decade of energy ($2.44/\ln(10)$). The factor of $N_{\nu} = 3$ converts the tau neutrino sensitivity to the all-flavor energy-squared scaled fluence $E_{\nu}^2 \phi_{\nu}$. As discussed above, the factor f_t decreases the time averaged area because of the impact of the Sun and the Moon on the observing time.

The sensitivity for long bursts is shown in Fig. 2 using $f_t = 0.3$ as an approximate derating of the average area due to the Sun and Moon. The dark band in Fig. 2 shows POEMMA's range of sensitivity for most of the sky. For example, for a given orbital position, over one orbit, the locations where this range of sensitivity applies is the region between the dashed curves in upper panel of Fig. 1. The extended purple band that includes the light shading shows the full range of the time-averaged sensitivity as a function of the tau neutrino energy. We show the IceCube, Auger and ANTARES per-flavor upper limit, multiplied by three for the all-flavor comparison. These limits are for a 14 day window following the trigger on GW170817 [61]. We also include two examples of long duration all-flavor fluences, the binary neutron star merger model of Fang and Metzger [21] scaled to a source distance of 10 Mpc and a blazar flare model of Rodrigues, Fedynitch, Gao, Boncioli and Winter (BFGBW) [19] scaled to a source distance of 25 Mpc.

The all-flavor sensitivity is plotted in Fig. 3 in galactic celestial coordinates for two fixed incident tau neutrino energies, 10^8 GeV and 10^9 GeV , where the position dependent f_t in Fig. 1 is also included. The minimum and maximum all-flavor sensitivities, assuming equal fluxes for the three neutrino flavors, are listed in Table I for $E_{\nu} = 10^8, 10^9$ and 10^{10} GeV .

For short bursts, the timing of the burst determines the extent to which POEMMA will be able to make observations. In the optimal location for a given time, the sensitivity to short bursts is better than for long bursts. For a source in POEMMA's field of view, behind the Earth with neutrinos that emerge in the range of $\beta_{\text{tr}} = 1^\circ - 35^\circ$, the optimal sensitivity is obtained by finding the time averaged effective area, now with $T_0 = 10^3 \text{ s}$. This best case scenario, both in terms of positioning of the source

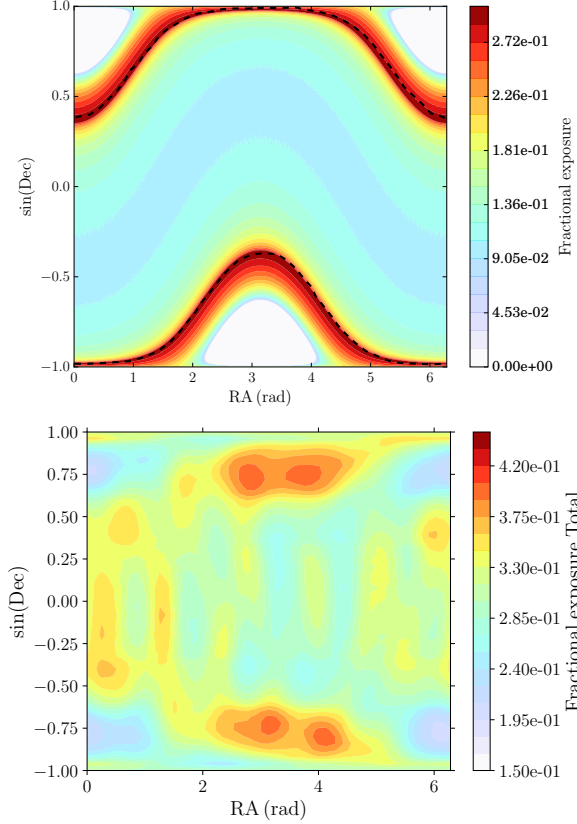


FIG. 1. Upper: Over one orbital period T_s , the sky coverage for sources at a given orbital position in the sine of the declination and right ascension, without including the effect of the Sun and Moon, at a given time of the year for viewing angles to $\delta = 18.3^\circ$ below the limb [55]. Lower: The fraction f_t of the the orbital period in which the source is not observable due to the Sun and Moon combined, as a function of source location in equatorial coordinates. The fractions come from an average over 7 precession periods of POEMMA’s orbital plane, namely, $7 \times 54.3 \text{ days} \simeq 380 \text{ days}$.

relative to POEMMA and the Earth and when the Sun and Moon do not interfere, is shown in Fig. 4. For this evaluation, we have taken $T_0 = 10^3 \text{ s}$, and started the viewing just as the source moves below the limb of the Earth. Figures 2 and 4 show that the time averaged sensitivity for long bursts and best case sensitivity for short bursts are close to two orders of magnitude better than the Auger limits. A key feature of these satellite-based instruments is that it can track the source of skimming tau neutrinos for a wider range of angles ($\beta_{\text{tr}} < 35^\circ$) than the ground-based Pierre Auger Observatory’s capability to observe Earth-skimming events ($\beta_{\text{tr}} < 6^\circ$) [43].

The source location dependent optimal sensitivities are shown for $E_\nu = 10^8 \text{ GeV}$ and 10^9 GeV , translated to all-flavor sensitivities, in Fig. 5. Min-

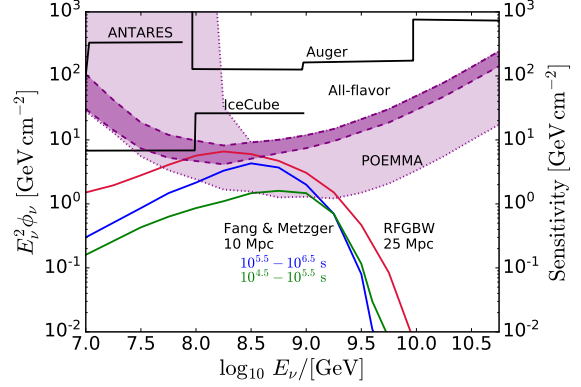


FIG. 2. The POEMMA all-flavor 90% unified confidence level sensitivity for a decade in energy in the purple band, compared with the IceCube, Auger and ANTARES sensitivities, scaled to 3 flavors, for 14 days after the trigger time of GW170817 [61]. Bounds set over an e-fold energy interval [62] are a factor of 2.3 less restrictive. Also plotted are two examples of long burst models: the all flavor fluence from a model of binary neutron star merger to millisecond magnetar with a source distance of $D = 10 \text{ Mpc}$ [21] and the RFGBW model of a blazar flare with proton advection at a distance of 25 Mpc [19]. The effects of the Sun and Moon in reducing the effective area are incorporated using a factor of $f_t = 0.3$.

imum and maximum sensitivities based on location for this best-possible short burst observations are listed in Table II. Even if POEMMA is not pointing at the burst, with an alert, POEMMA can slew 90° in 500 s. For most locations, a 500 s delay will not change the sensitivity to 10^3 s bursts if the source alignment with the Earth is optimal, since the burst duration is longer than the amount of time the source is visible to POEMMA (see Fig. 6).

This last feature, and the result that POEMMA is potentially more sensitive to well-positioned neutrino sources with short bursts than to long bursts, can be seen in Fig. 6. For this example, we consider sources that are at equatorial RA of 0° where a line from the Earth to the source is at an angle of θ_i relative to POEMMA’s orbital plane. All other source locations can be mapped to this configuration if we are free to choose t_0 in Eq. (6).

The green shaded band in Fig. 6 shows the fraction of an orbit period T_s when a source is behind the Earth in a line of elevation angle $\beta_{\text{tr}} = 1^\circ - 35^\circ$ first setting below the horizon, then rising about the limb of the Earth as viewed from the POEMMA satellites. For example, for $\theta_i = 0^\circ$, the source is in the orbital plane. For two time intervals (the two green shaded intervals), the source is behind the Earth with angles of $\beta_{\text{tr}} = 1^\circ - 35^\circ$. The region between the green bands represents the time when the neutrino fluence is strongly attenuated. Before

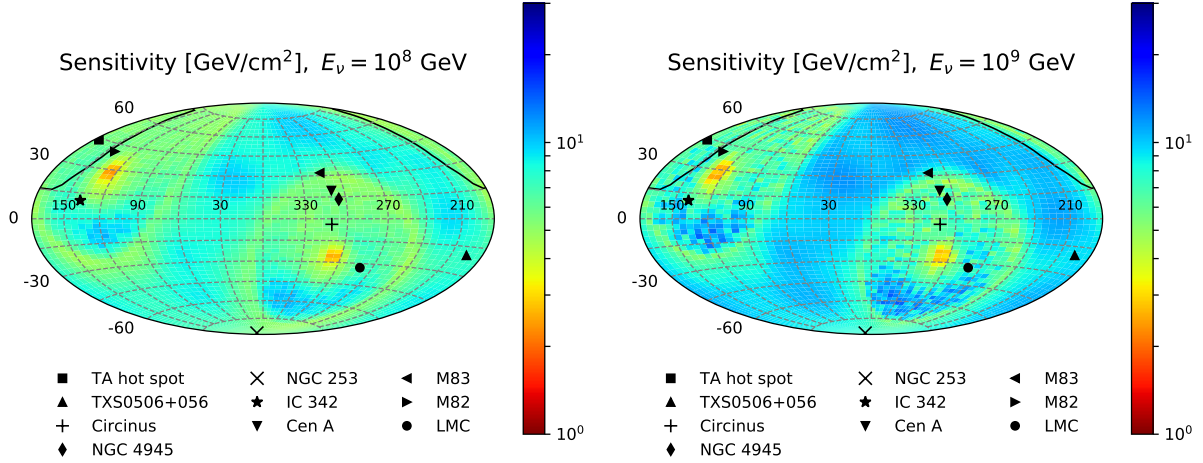


FIG. 3. The all-flavor 90% unified confidence level sensitivity, for $E_\nu = 10^8$ GeV (left) and 10^9 GeV (right), for long bursts with a factor of f_i from the corrections in Fig. 1 for the time-averaged effective area, in galactic coordinates in a Hammer projection. Selected sources are shown, including: (i) the Telescope Array’s (TA) “hot spot” with a spherical cap of radius 28.43° [63, 64], (ii) nearby starburst galaxies featuring a possible correlation with UHECRs [65–67], (iii) the closest radiogalaxy Centaurus A (Cen A), (iv) the blazar observed by IceCube [3, 68], and (v) the Large Magellanic Cloud (LMC).

the first green interval and after the second interval, the source is not behind the Earth. For $\theta_i \simeq 50^\circ$, the source dips below the horizon but $\beta_{tr} \leq 35^\circ$. Given the inclination of POEMMA’s orbital plane of 28.5° , when $\theta_i > 68.5^\circ$, the source is never below the Earth’s horizon for POEMMA. In Figs. 2 and 4, the dashed lines bracket the sensitivities (including the effect of the Sun and Moon for long bursts) for $\theta_i \leq 50^\circ$ (the dark purple region), and the dotted lines extend to $50^\circ < \theta_i < 67.5^\circ$ with the light purple region.

For long bursts, $\langle A(E_\nu) \rangle$ is determined with T_s , the full range of the y -axis in Fig. 6. For short bursts, the fraction of the y -axis equivalent to 10^3 s is shown with the pink band. The time average of the effective area is the probability weighted green band with normalization of 10^3 s. If the burst begins at $t = 0$ for $\theta_i = 0^\circ$, a 10^3 s burst will not be observed at all. On the other hand, if the burst begins within $\sim 500 - 700$ s of the viewing window, either green band, the sensitivity is the optimal value. This is true for most of the angles θ_i . The dark pink band shows a window of 500 s. If the source is optimally placed, a 500 s delay from slewing the instrument to the position of the source will not change the sensitivity.

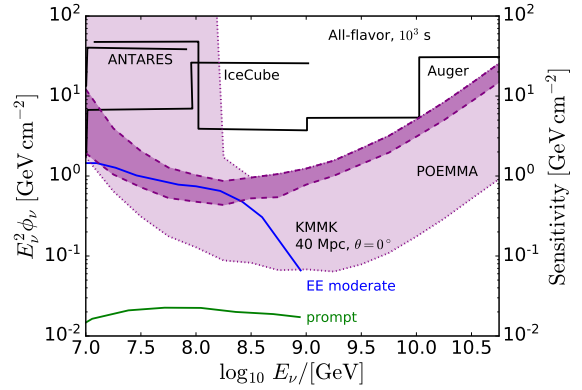


FIG. 4. The POEMMA target of opportunity all-flavor 90% unified confidence level sensitivity for a decade in energy. The purple band shows the range of sensitivities accessible to POEMMA for a 10^3 s burst. The dark purple band corresponds to source locations in a large portion of the sky. The IceCube, Auger and ANTARES sensitivities, scaled to 3 flavors, for ± 500 s around the binary neutrino star merger GW170817 are shown with solid histograms [61]. Also plotted is an example of a short neutrino burst, the Kimura, Murase, Mészáros and Kiuchi (KMMK) [16] all flavor fluence for extended emission and prompt emission from a short gamma ray burst, scaled to 40 Mpc, for on-axis viewing ($\theta = 0^\circ$).

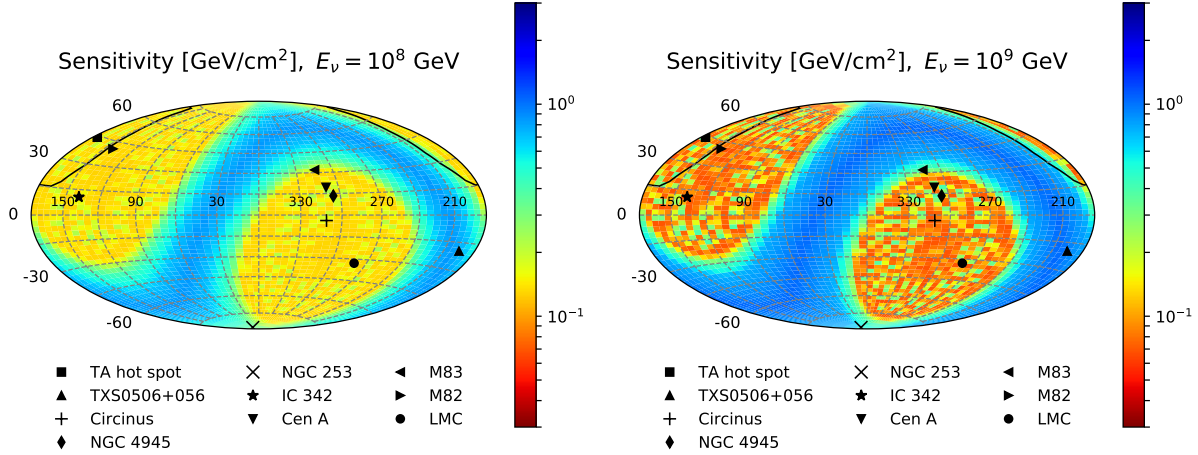


FIG. 5. The all-flavor 90% unified confidence level maximum sensitivity over a single POEMMA orbit during a 380-day period for short (10^3 s) bursts, assuming optimal viewing conditions for the burst, for $E_\nu = 10^8$ GeV (left) and 10^9 GeV (right). Figures show the Hammer projection in galactic coordinates, with the sensitivity in units GeV/cm^2 .

TABLE I. Long bursts, minimum and maximum best all-flavor sensitivity at 90% unified confidence level, in units of $[\text{GeV}/\text{cm}^2]$ assuming f_t from 380-day averages from Fig. 1.

E_ν [GeV]	min	max
10^7	55.9	3.90×10^3
10^8	2.34	10.8
10^9	2.49	14.6
10^{10}	11.6	61.3

TABLE II. Bursts of 10^3 s, minimum and maximum best all-flavor sensitivity in astronomical night ($f_t = 1$) at 90% unified confidence level, in units of $[\text{GeV}/\text{cm}^2]$.

E_ν [GeV]	min	max
10^7	1.72	42.6
10^8	1.28×10^{-1}	8.49×10^{-1}
10^9	6.81×10^{-2}	1.05
10^{10}	1.76×10^{-1}	4.30

III. NEUTRINO ESTIMATES FROM FLARING ASTROPHYSICAL SOURCES AND NEUTRINO HORIZONS

In this section, we use the position-dependent effective area to calculate the expected number of neutrino events that would be detectable by POEMMA for several models of astrophysical transients at var-

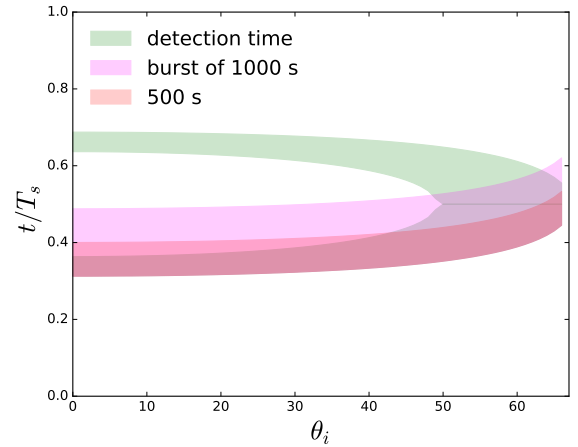


FIG. 6. The green band show the fraction of the time during which the source is observable during astronomical night relative to the orbital period for a given θ_i (see text). The pink band shows the burst time of 10^3 s relative to the orbital period of $T_s = 5,700$ s. The red band show the relative time of 500 s to T_s .

ious distances. Additionally, we calculate the neutrino horizon, which is the maximum distance at which POEMMA will be able to detect neutrinos, for each source model. As the nearby matter distribution is fairly anisotropic, we begin with a discussion of our methodology for determining the galaxy-luminosity weighted effective area that we use to calculate the number of neutrino events and the neutrino horizons. Included in this section is a discussion of a range of models of transient neutrino sources. We summarize our results in Table III.

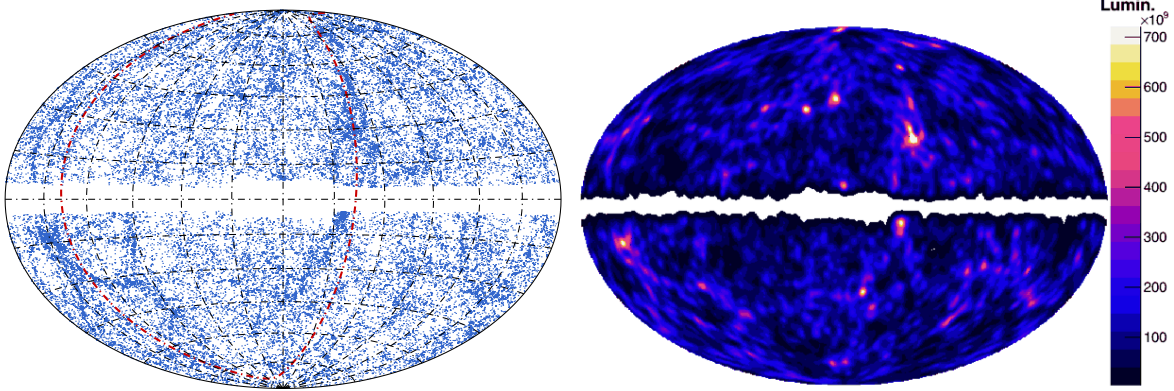


FIG. 7. *Left*: Sky plot of galaxies in the 2MRS catalog. Overdensities seen in the plot are due to nearby clusters of galaxies. For reference, the supergalactic plane is plotted as the red dot-dashed line. *Right*: Sky plot of the 2MRS catalog weighted by galaxy luminosity and smoothed with a Gaussian, in units of L_0 .

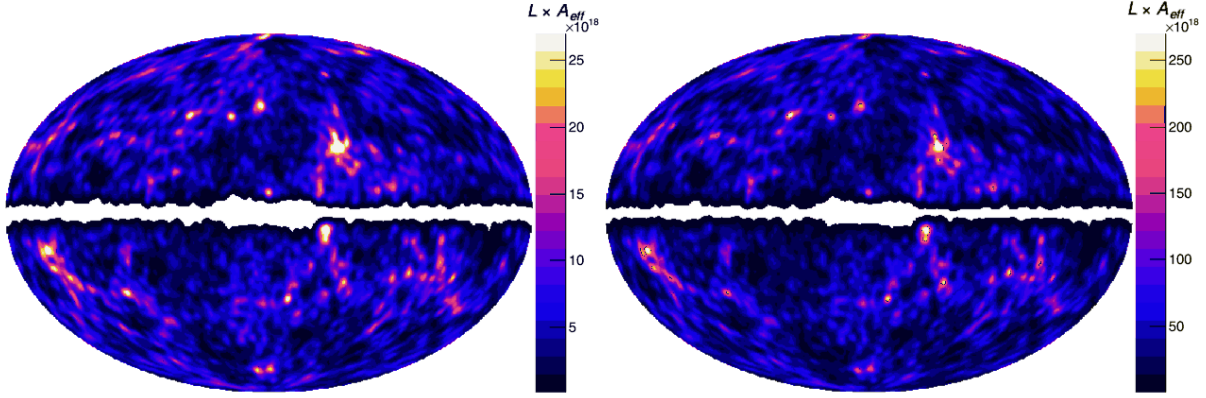


FIG. 8. *Left*: Sky plot of the smoothed 2MRS catalog galaxy luminosity weighted effective area in units of $L_0 \cdot \text{cm}^2$ for $E_{\nu_\tau} = 10^8$ GeV for long bursts. *Right*: As at left, for $E_{\nu_\tau} = 10^9$ GeV for long bursts.

A. Effective Area Averaged Over the Sky

As evidenced in Figs. 3 and 5, the effective area of POEMMA varies considerably over the sky due to the orbital characteristics of the satellites and the influence of the Sun and the Moon (see Sec. II). To calculate the expected numbers of neutrinos from models of astrophysical neutrino sources, we compute the average effective area over the sky as a function of redshift:

$$\mathcal{A}(E_\nu, z) = \frac{\int \langle A(E_\nu, \theta, \phi) \rangle_{T_0} p(\theta, \phi, z) d\Omega}{\int p(\theta, \phi, z) d\Omega}, \quad (8)$$

where $p(\theta, \phi, z)$ is the weighting function expressing the probability of finding a source at a given position, (θ, ϕ) , where $\theta = \frac{\pi}{2} - b$ and $\phi = l$ are expressed in galactic longitude and latitude, (l, b) and and $d\Omega = \sin \theta d\theta d\phi$, at a given redshift, z .

The weighting function is determined by the distribution of matter in the universe, which while be-

ing statistically isotropic out to high redshifts, is relatively anisotropic out to the distances within which POEMMA is most likely to detect neutrinos. As such, we model the weighting function using the 2MASS Redshift Survey (2MRS) of galaxies in the nearby universe (see Fig. 7) [69]. The 2MRS catalog includes a sample of nearly 45,000 galaxies selected from the original 2 Micron All-Sky Survey (2MASS) [70]. The resulting 2MRS redshift catalog consists of galaxies with apparent magnitudes $K_s \leq 11.75$ mag in the near infrared and galactic latitudes $|b| \geq 5$ degrees ($|b| \geq 8$ degrees near the Galactic bulge). Galaxy redshifts are provided as measured radial velocities in the solar system barycenter reference frame. In order to compute cosmological redshifts for each galaxy, radial velocities are corrected to the cosmic microwave background (CMB) reference

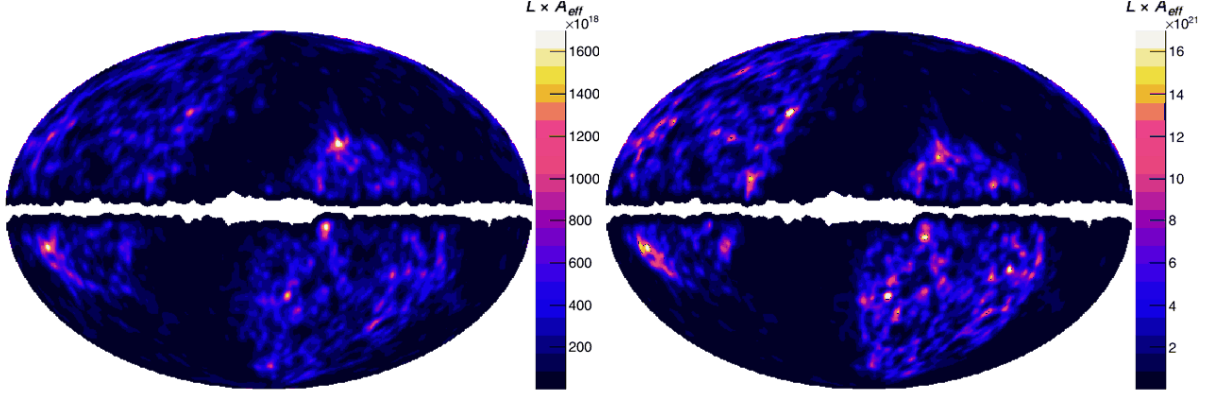


FIG. 9. *Left*: Sky plot of the smoothed 2MRS catalog galaxy luminosity weighted effective area in units of $L_0 \cdot \text{cm}^2$ for $E_{\nu_\tau} = 10^8$ GeV for short bursts. *Right*: As at left, for $E_{\nu_\tau} = 10^9$ GeV for short bursts.

frame through

$$V_{\text{corr}} = V_{\text{uncorr}} + V_{\text{apex}} \sin(b) \sin(b_{\text{apex}}) + V_{\text{apex}} \cos(b) \cos(b_{\text{apex}}) \cos(l - l_{\text{apex}}), \quad (9)$$

where $l_{\text{apex}} = 264.14$ degrees, $b_{\text{apex}} = +48.26$ degrees, and $V_{\text{apex}} = 371.0 \text{ km s}^{-1}$, which accounts for the motion of the Galaxy with respect to the CMB [71]. For those 2MRS galaxies with positive corrected radial velocities, redshifts are then determined using

$$V_{\text{rad}} = V_{\text{corr}} = c \int_0^z \frac{dz'}{E(z')}, \quad (10)$$

where $E(z') = \sqrt{\Omega_M (1+z')^3 + \Omega_k (1+z')^2 + \Omega_\Lambda}$ with $(\Omega_M, \Omega_k, \Omega_\Lambda)$ being cosmological parameters related to the matter density of the universe, the curvature of the universe, and the dark energy density, respectively (*c.f.*, Refs. [72–74]).¹ For those 2MRS galaxies with negative corrected radial velocities (only 25 galaxies out of the full sample), rather than using redshifts, we instead determine their distances by following a procedure similar to that discussed in Ref. [77]. Most of the 2MRS galaxies have been associated with known nearby galaxies, and distances are provided in the Extragalactic Distance Database (EDD) [78]. For the four 2MRS galaxies that remain unassociated, we used the distances of their nearest neighbors from the list of 25 2MRS galaxies with negative corrected radial velocities.

¹ For this paper, we take $\Omega_M = 0.3153$, $\Omega_\Lambda = 0.6847$, $\Omega_k = 1 - (\Omega_M + \Omega_\Lambda) = 0$, and $H_0 = 67.36 \text{ km s}^{-1} \text{ Mpc}^{-1}$ [75]. We have verified that if we adopt the value of H_0 derived from the maser-cepheid-supernovae distance ladder [76] our results are not significantly altered.

With redshifts or distances associated with every galaxy in the 2MRS catalog, we construct maps of the weighting function in bins of redshift. In so doing, we consider two options for assigning weights to the galaxies in the catalog: (1) assigning the same weight to every galaxy; (2) weighting each galaxy according to its luminosity. Galaxy luminosities, L , are computed from their absolute magnitudes, M by

$$\frac{L}{L_0} = 10^{-0.4M}, \quad (11)$$

where L_0 is the zero-point luminosity in the K_s bandpass (taken to be the luminosity of Vega in the K_s band). The absolute magnitude is computed from K_s apparent magnitudes using

$$M = m + \Delta m - A_K(l, b) - k(z) - e(z) - DM(z), \quad (12)$$

where m is the apparent magnitude in the K_s bandpass, $\Delta m = 0.017$ is the zero-point offset required to calibrate the 2MASS with the standard Vega system [79], $A_K(l, b)$ is the correction for extinction due to dust in the Milky Way (already included in 2MRS apparent magnitudes), $k(z)$ is the k-correction due to cosmological redshifting of the spectrum, $e(z)$ corrects for evolution in galaxy spectra arising from stellar populations aging over the redshift distribution of the survey [80],

$$DM(z) = 5 \log_{10} \left(\frac{d_L}{10 \text{ pc}} \right) \quad (13)$$

is the distance modulus, and

$$d_L = \frac{c}{H_0} (1+z) \int_0^z \frac{dz'}{E(z')} \quad (14)$$

is the luminosity distance. For the k- and evolution-corrections, we adopt the values given in Ref. [81]:

$$k(z) = -2.1z \quad (15)$$

$$e(z) = 0.8z. \quad (16)$$

TABLE III. Expected numbers of neutrino events above $E_\nu > 10^7$ GeV detectable by POEMMA for several models of transient source classes assuming source locations at the galactic center (GC) and at 3 Mpc. The horizon distance for detecting 1.0 neutrino per ToO event is also provided. Source classes with observed durations $> 10^3$ s are classified as long bursts. Those with observed durations $\lesssim 10^3$ s are classified as short bursts. Models in boldface type are those models for which POEMMA can expect at least one ToO in ~ 25 years of operation.

Long Bursts				
Source Class	No. of ν 's at GC	No. of ν 's at 3 Mpc	Largest Distance for 1.0 ν per event	Model Reference
TDEs	1.12×10^5	0.77	2.64 Mpc	Dai and Fang [17] average
TDEs	5.62×10^5	3.88	5.91 Mpc	Dai and Fang [17] bright
TDEs	2.23×10^8	1.44×10^3	115.20 Mpc	Lunardini and Winter [18] $M_{\text{SMBH}} = 5 \times 10^6 M_\odot$ Lumi Scaling Case
TDEs	NA*	1.07×10^3	100.03 Mpc	Lunardini and Winter [18] $M_{\text{SMBH}} = 1 \times 10^5 M_\odot$ Strong Scaling Case
Blazar Flares	NA*	1.91×10^2	42.96 Mpc	RFGBW [19] – FSRQ proton-dominated advective escape model
IGRB Reverse Shock (ISM)	9.88×10^4	0.69	2.49 Mpc	Murase [15]
IGRB Reverse Shock (wind)	2.05×10^7	143.75	37.36 Mpc	Murase [15]
BH-BH merger	6.94×10^6	47.84	20.75 Mpc	Kotera and Silk [20] – $t_{\text{dur}} \sim 10^4$ s
BH-BH merger	3.48×10^9	2.4×10^4	477.8 Mpc	Kotera and Silk [20] – $t_{\text{dur}} \sim 10^{6.7}$ s
NS-NS merger	3.58×10^6	24.75	12.76 Mpc	Fang and Metzger [21]
WD-WD merger	20.06	0	33.46 kpc	XMMD [22]
Newly-born Crab-like pulsars (p)	1.56×10^2	1.07×10^{-3}	98.27 kpc	Fang [23]
Newly-born magnetars (p)	2.1×10^4	0.13	1.1 Mpc	Fang [23]
Newly-born magnetars (Fe)	4.07×10^4	0.26	1.53 Mpc	Fang [23]
Short Bursts				
Source Class	No. of ν 's at GC	No. of ν 's at 3 Mpc	Largest Distance for 1.0 ν per event	Model Reference
sGRB Extended Emission (moderate)	2.23×10^8	1.55×10^3	117.44 Mpc	KMMK [16]
sGRB Prompt	8.10×10^6	69.19	26.66 Mpc	KMMK [16]

(*) Not applicable due to mismatch with mass of SMBH at the GC and/or lack of blazar-like jet.

Many studies of redshift surveys such as the 2MRS make use of isophotal apparent magnitudes², which would require an aperture correction that would convert these observed aperture magnitudes to some proper diameter (*c.f.*, Ref. [77]). For our study, we use the extrapolated total apparent magnitudes provided in the 2MRS catalog; hence, the aperture correction is not needed [77, 82].

In addition to enabling the calculation of galaxy luminosities, the calculated absolute magnitudes also enabled the construction of volume-limited samples in every redshift bin. In each bin, we calculated the limiting absolute magnitude for which a galaxy at the highest redshift in the bin would have an observed apparent magnitude at the survey limit (*i.e.*, $K_s = 11.75$ mag). We then included only those galaxies with calculated absolute magnitudes that were less than the limiting absolute magnitude for that bin. This corrects for the possible bias in favor of fainter galaxies that could only be detected at the lower redshifts in the bin.

Finally, the weighting function maps are created by smoothing our constructed 2MRS samples with a Gaussian with $\sigma = \theta_{\text{Ch}}^{\text{app}} / \sqrt{2 \ln 2}$, where $\theta_{\text{Ch}}^{\text{app}} \sim 1.5^\circ$ is an approximation of the effective Cherenkov angle. The effective area averaged over the constructed weighting functions is then calculated for each redshift bin according to Eq. (8). Sample maps for the entire 2MRS catalog are provided in Figs. 8 and 9.

B. Expected Numbers of Neutrino Events from Modeled Astrophysical Neutrino Fluences

With the average effective area computed as a function of energy and redshift, the expected number of neutrino events from an astrophysical source at redshift z is given by

$$N_{\text{ev}} = \int_{\Delta E_\nu} \phi_{\nu_\tau}(E_\nu) \mathcal{A}(E_\nu, z) dE_\nu, \quad (17)$$

where $\phi_{\nu_\tau}(E_\nu)$ is the single-flavor ($N_\nu = 1$) neutrino fluence in units of energy per unit area. The observed energy-squared scaled tau-neutrino fluence is given by

$$E_\nu^2 \phi_{\nu_\tau}(E_\nu) = \frac{(1+z)}{4\pi d_L^2} \frac{Q}{3} E_{\text{src}}^2 \Delta t_{\text{src}}, \quad (18)$$

where Q is the (all flavor) neutrino source emission rate as measured by a fundamental observer at the

source redshift in units of neutrinos per energy interval per time interval, Δt_{src} is the event duration at the source redshift, E_{src} is the emission energy, and we assume that relevant quantities for calculating the fluences, are *isotropic equivalent* quantities (for derivation of Eq. (18), see Appendix B) and that neutrino oscillations yield equal flavor ratios on Earth. For any astrophysical model that provides an observed fluence for a source at a given redshift or luminosity distance, the observed fluence can be computed for any redshift using Eq. (18) by calculating the intrinsic neutrino source emission rate and then rescaling to the new redshift. The expected number of neutrino events predicted by the astrophysical model for a source at z is then given by Eq. (17). The neutrino horizon, z_{hor} , for a specific astrophysical model can also be calculated from Eq. (17) by determining the redshift at which N_{ev} is equal to a given value. In this study, we set $N_{\text{ev}} = 1.0$.

In Table III, we provide the calculated number of neutrino events for several models of astrophysical transient source classes assuming a source at the Galactic Center and at 3 Mpc (roughly the distance to the nearest starburst galaxy, NGC253). To provide a sense of the maximum distance at which a given source class is detectable by POEMMA, we include its neutrino horizon expressed as a luminosity distance as determined from a model taken from the literature. In Fig. 10, we plot the horizons as a function of position on the sky for three of the models (two of which are for long duration models and one of which is for a short duration model) to demonstrate the variation in the horizon with the variation in the sensitivity of POEMMA.

For long bursts with durations $> 10^3$ s, the average impacts of the Sun and the Moon have been included in the calculation of the average effective area; hence, the results in Table III for long bursts should be considered averages. For short bursts with durations $\sim 10^3$ s, the effects of the Sun and the Moon vary strongly over the course of the orbital period of the POEMMA satellites, and the number of possible configurations is large. As such, we do not include the effects of the Sun and the Moon in the average effective area for short bursts, and in these cases, the results in Table III should be considered upper limits.

In the remainder of this section, we provide summaries of the various astrophysical neutrino fluence models and how to interpret the corresponding results included in Table III. We begin this discussion with the source classes that are most likely to result in at least one ToO in ~ 25 years of observations with POEMMA as determined by their neutrino horizons provided in Table III and cosmological event rates provided in the literature. These

² *I.e.*, from fluxes integrated within the isophotal radius, the distance from the center along the semi-major axis beyond which the surface brightness falls below a given value.

models are denoted in Table III using boldface type. We conclude the section with a discussion of source classes that would be detectable by POEMMA if located reasonably close by, but for which expectations for their neutrino horizons and estimates of their cosmological event rates imply ToO rates that would require more than 25 years of observations with POEMMA in order to detect one event. Based on the results from this study and studies of ToOs with other neutrino observatories provided in the literature, we expect these sources to be challenging to observe by any currently operating or planned neutrino observatories.

1. Most Favorable Transient Source Classes for Targets of Opportunity with POEMMA

— *Blazar Flares* — Active galactic nuclei (AGNs) are the most luminous persistent sources in the universe, powered by accretion onto SMBHs with masses ranging up to $\sim 10^{10} M_\odot$. Accretion of highly magnetized plasma by the SMBH can launch powerful, relativistic jets that are capable of accelerating particles to high energies and possibly beyond [For a recent review of relativistic jets in AGNs, see 83]. As they possess the characteristics necessary to accelerate particles to ultra-high energies (*i.e.*, they possess the magnetic field strengths and spatial scales required to confine particles until they reach energies $\gtrsim 10^{18}$ eV; see *e.g.*, 84, 85), AGN jets have long been proposed as candidate sources of the highest energy cosmic rays [86, 87]; though, giant radio lobes and termination shock hot spots observed in some AGN morphologies have also been suggested [see *e.g.*, 88–92]. High radiation levels expected to be present in AGN jets would naturally give rise to high-energy neutrinos as protons and nuclei that are accelerated to ultra-high energies experience catastrophic losses via photomeson interactions [see *e.g.*, 93, 94]. As such, AGN jets have long been regarded as promising neutrino sources with blazars, those AGN with a jet aligned with the line-of-sight of the observer, being the most attractive candidates for searches due to relativistic Doppler boosting. The recent IceCube detection of a high-energy neutrino ($E \gtrsim 300$ TeV) temporally and spatially coincident with a gamma-ray flare from blazar TXS 0506+056 [3] and the identification of a prior neutrino flare from the same source [68] provided the strongest evidence to date that AGNs produce neutrinos, as well as providing the first clues into the origins of the astrophysical neutrino flux and hints into the acceleration of hadrons to very-high energies and possibly beyond.

Neutrino production in AGN jets has been extensively discussed in the literature [see *e.g.*, 19, 93–

113]. In Ref. [19], RFGBW performed an extensive parameter study modeling the acceleration, transport, and interactions of CR nuclei in blazar flares and their resulting neutrino, gamma-ray, and UHECR spectra. RFGBW injected various nuclear isotopes and then modeled their evolution according to the transport equation, allowing for nuclear disintegration, cooling via pair production and photomeson production, and escape losses via advection or diffusion. For the purposes of evaluating the capability of POEMMA to observe neutrinos from blazar flares, we adopt their pure proton composition model for a high-luminosity blazar assuming escape via advection for CRs. In these models, advective escape allows for more CRs to escape to the broad-line and dusty torus regions of the AGN where they have more time to interact with photon fields and produce neutrinos; as such, neutrino fluences in these models are enhanced (with respect to the diffusive escape models), particularly at the higher energies (tens of PeV and above). As noted in Table III, we can expect POEMMA to detect \sim tens – hundreds of neutrino events for nearby, powerful blazars assuming this model.³ The neutrino horizon for POEMMA for this model is ~ 43 Mpc, indicating that POEMMA can detect such blazars out to reasonable distances. Models with heavier nuclei or mixed compositions will produce fewer neutrinos and closer horizons, but such scenarios may still be observable for sufficiently nearby events.

In order to determine the number of ToO events expected in 25 years of observations by POEMMA, we must calculate the cosmological rate of blazar flares. To that end, we determine the cosmological rate from the cosmological density of blazars and estimates of the frequency of flares. For the cosmological density of blazars, we adopt the local value of $\sim 1.5 \times 10^{-7}$ Mpc $^{-3}$ from Ref. [114]. The frequency of flares is determined by the fraction of time that a blazar is in the flaring state, the so-called “duty cycle.” The value of the blazar duty cycle and blazar variability, in general, has been the subject of considerable debate in the literature [see *e.g.*, 115–118]. Any effect that would result in variation in the emission from a given blazar (*e.g.*, jet precession, instabilities in the jet flow, variations in the supermassive black hole accretion rate, or similar effects) would presumably contribute to its duty cycle. Such blazar characteristics are subject to a considerable degree of uncertainty, and it is as yet unclear whether a single parameter such as the duty

³ Due to the lack of a powerful blazar-like jet at the GC, we do not provide numbers for a source at the GC for this model.

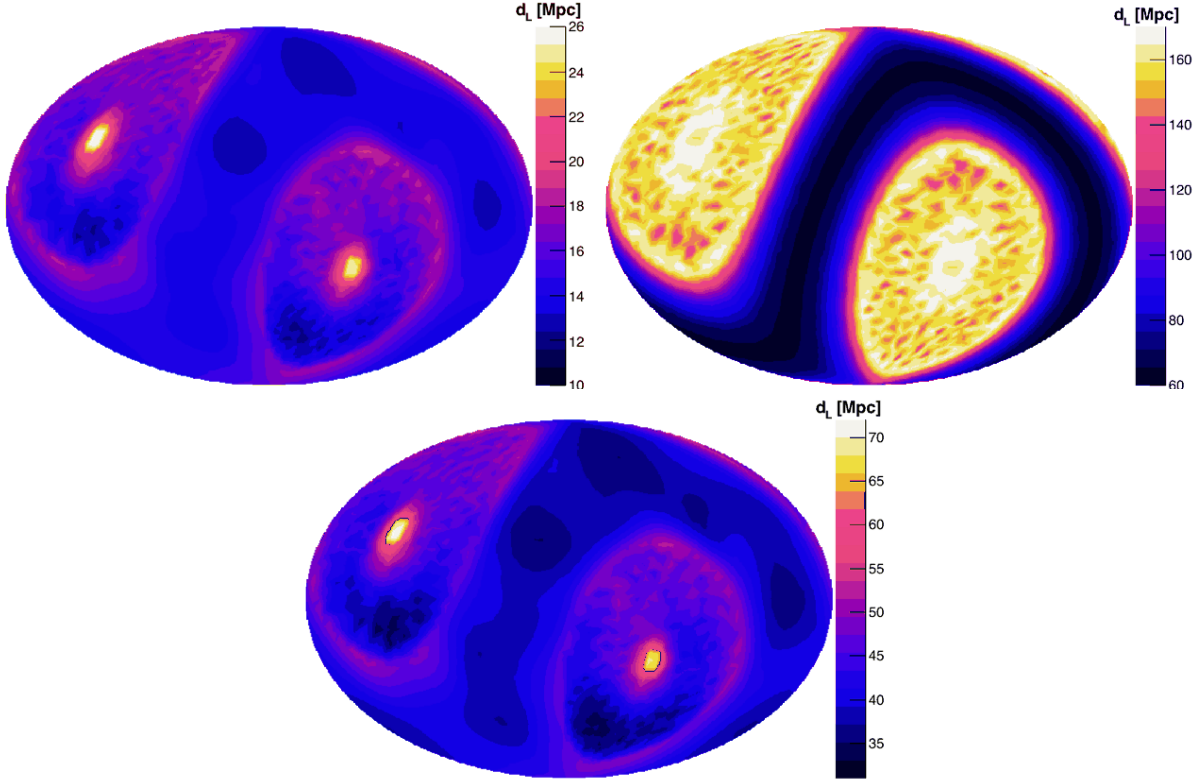


FIG. 10. *Top Left:* Sky plot of the neutrino horizon for the NS-NS merger model of Ref. [21]. *Top Right:* Same as at left for the sGRB EE neutrino model of Ref. [16]. *Bottom:* Same as at top for the blazar flare model of Ref. [19]

cycle can adequately reflect the complexities of the variation in blazar emission. For the purposes of this discussion, we take the relatively conservative estimates of $\sim 1\text{--}10\%$ for the blazar duty cycle. These values correspond to $\sim 3\text{--}30$ flares per year per blazar for flare time scales on the order of hours, and the resulting cosmological rate of blazar flares is $\mathcal{R} \sim 4.5\text{--}45 \times 10^{-7} \text{ Mpc}^{-3} \text{ yr}^{-1}$. Adopting the neutrino horizon of $\sim 43 \text{ Mpc}$ for the pure proton advective escape model, we expect the ToO rate for blazar flares for POEMMA to be ~ 1 event per few years to $\gtrsim 1$ per year. If we take $\sim 50\%$ for the duty cycle (consistent with the mean value for the blazar population; [118]), the ToO rate would be ~ 1 – a few events per year with POEMMA.

— *Jetted Tidal Disruption Events* — A TDE occurs when a star orbiting a massive black hole approaches close enough for the star to be ripped apart by the tidal forces of the black hole [119, 120; for detailed reviews, see *e.g.*, [121, 122]. While some of the stellar material will be ejected from the system, much of it will be accreted onto the black hole resulting in a flare of thermal radiation that peaks in the ultraviolet or soft X-rays [120, 123, 124] and declines on timescales of \sim months to years [125, 126]. The discovery of the TDE Swift J1644+57 by the *Neil*

Gehrels Swift Observatory Burst Alert Telescope [127] demonstrated that at least some TDEs launch powerful, relativistic jets that emit non-thermal radiation [128–130]. With the capability of launching relativistic jets and the abundance of baryons from the disrupted stellar material, it is natural to consider the possibility that TDEs could accelerate protons and nuclei, possibly even up to ultra-high energies [131–133]. Photomeson interactions between accelerated protons and nuclei and thermal and non-thermal radiation will give rise to very-high and ultra-high energy neutrinos that could be detected by neutrino telescopes [17, 18, 134, 135].

In order to evaluate the capability of POEMMA for detecting neutrinos from jetted tidal disruption events, we adopt the model of Lunardini and Winter Ref. [18]. We calculate the expected numbers of neutrino events and neutrino horizons assuming different model parameters. Alternative models of neutrino production in TDEs available in the literature yield comparable results [*e.g.*, [134–137]. In Ref. [18], Lunardini and Winter performed a detailed study of neutrino fluences from jetted TDEs for various assumptions about the scalings relating key jet characteristics (*i.e.*, bulk Lorentz factor, variability timescale, and X-ray luminosity) to the mass

of the SMBH. For our calculations of the number of neutrino events and the neutrino horizons for POEMMA, we consider two models from Ref. [18]: a Strong Scaling model with $M_{\text{SMBH}} = 10^5 M_\odot$ and a Lumi Scaling model with $M_{\text{SMBH}} = 5 \times 10^6 M_\odot$. In the Strong Scaling Model, the jet bulk Lorentz factor and the variability timescale scale with SMBH mass resulting in a pion production efficiency that is inversely proportional to a power of the SMBH mass, $f_{p\gamma} \propto \Gamma^{-4} t_v^{-1} \propto M_{\text{SMBH}}^{-1.8}$ [18; see also, 14, 138]; hence, in this class of models, lower SMBH masses result in higher neutrino fluences. The Lumi Scaling model includes the further assumption that the X-ray luminosity is proportional to the SMBH mass ($L_X \propto M_{\text{SMBH}}$), resulting in a neutrino fluence that is related to the SMBH mass according to $\phi \propto L_X f_{p\gamma} \propto L_X^2 M_{\text{SMBH}}^{-1.8} \propto M_{\text{SMBH}}^{0.2}$ after accounting for the dependence of the pion production efficiency on the X-ray luminosity. For the more massive SMBH model, the value of $5 \times 10^6 M_\odot$ was motivated by estimates of the mass of Sgr A* [see *e.g.*, 139], and the neutrino fluence was determined by interpolating between the $10^6 M_\odot$ and the $10^7 M_\odot$ Lumi Scaling models in Ref. [18]. As such, this model provides expectations for POEMMA observations in the event of a TDE involving the SMBH at the galactic center (GC), demonstrating that POEMMA will detect $\sim 2 \times 10^8$ neutrinos in such a scenario. For the $10^5 M_\odot$ model, the number of neutrino events were not calculated for a TDE at the GC due to mismatch with the mass of Sgr A*. In addition to the neutrino fluence, Lunardini and Winter [18] also modeled the cosmological rate of TDEs, finding the local rate of jetted TDEs to be $\mathcal{R} \simeq 0.35\text{--}10 \text{ Gpc}^{-3} \text{ yr}^{-1}$. For both the $10^5 M_\odot$ and $5 \times 10^6 M_\odot$ models considered in this work, the neutrino horizon is $\sim 100 \text{ Mpc}$, resulting in a ToO rate of $\gtrsim 1$ per 25 years of observation with POEMMA with higher rates possible for higher mass SMBHs in the Lumi Scaling Case.

— *Binary Neutron Star and Binary Black Hole Mergers* — Another class of sources that have been proposed as possible sources of UHECRs and neutrinos is that of pulsars, particularly rapidly spinning pulsars and magnetars [see *e.g.*, 140–144]. Strong magnetic fields and rapid rotation combine to induce electric fields that naturally accelerate particles. Ultra-high energies are achievable in magnetars (pulsars with magnetic field strengths $\gtrsim 10^{14} \text{ G}$; for detailed review, see Ref. 145) with spin periods \sim milliseconds [21]. With such strong magnetic fields, magnetic braking will quickly spin the magnetar down to periods \sim seconds [145], at which point CR energies would be limited to \sim PeVs. As such, the pulsars that are most likely to accelerate UHECRs are newly-born magnetars [see *e.g.*, 142–144]. Accelerated UHECRs produce neutrinos through in-

teractions with the surrounding ambient medium and radiation fields, the nature of which depends on the physical mechanism that led to the formation of the magnetar. In some cases, binary neutron star (BNS) mergers can result in a stable, rapidly spinning magnetar surrounded by low-density ejecta and a radiation field consisting of thermal photons from ionized ejecta and non-thermal photons from synchrotron and Inverse Compton radiation from ejected pairs [146]. In Ref. [21], Fang and Metzger modeled the time-dependent neutrino production arising from the interactions of UHECRs accelerated in the magnetar magnetosphere and the surrounding medium and radiation field characteristic of BNS mergers. Their model predicts that PeV–EeV neutrinos could be detectable for days and even months following the merger. Following the announcement of the observation of a BNS merger [1, 147] by Advanced LIGO [148] and Advanced Virgo [149], the ANTARES, IceCube, and Pierre Auger Observatories conducted a search for high-energy neutrinos positionally coincident with the merger arriving within $\pm 500 \text{ s}$ of the merger time and within a 14-day period following the merger [61]. No neutrinos were found, though at a distance of $\sim 40 \text{ Mpc}$, the neutrino fluences predicted by Fang and Metzger would have been undetectable with these neutrino experiments. As shown in Fig. 2, POEMMA will have an advantage in searching for neutrinos from BNS merger events due to its capability to rapidly re-point for follow-up and to revisit a source location every orbit and also due to the fact that POEMMA is most sensitive at the energies at which the neutrino fluences are expected to peak (\sim hundreds PeV). Using the Fang and Metzger model, we predict that POEMMA will be able to detect \sim tens of neutrinos up to distances \sim few Mpc. The predicted neutrino horizon for POEMMA for such events up is $\sim 13 \text{ Mpc}$. Based on this horizon and the event rate for BNS mergers provided by LIGO/Virgo of $\mathcal{R} \sim 110\text{--}3840 \text{ Gpc}^{-3} \text{ yr}^{-1}$ [150], we expect POEMMA to detect one such event in roughly 25 years of observation.

Analogous to BNS mergers, binary black hole (BBH) systems are also potential reservoirs of power. For instance, the rotational energy of a spinning black hole in a magnetized disk can be extracted to power jets [151]. However, unlike in the case of BNS mergers, black holes in BBH systems lack a companion that can be tidally disrupted and reorganized into an accretion disks [152]. As such, BBH mergers are generally expected to release energy solely in the form of gravitational waves. On the other hand, the tentative detection by the *Fermi* Gamma-ray Burst Monitor of a possible gamma-ray counterpart to the BBH merger GW150914 [153] has spurred interest

in scenarios that would result in an electromagnetic counterpart to a BBH merger, including the possibility of pre-existing material still being present at the time of the merger [see *e.g.*, 154–162] or the possibility of charged black holes [see *e.g.*, 163–166]. In Ref. [20], Kotera and Silk take the further step of suggesting that if BBH mergers can form accretion disks and associated jets or magnetohydrodynamic outflows, the CRs could be accelerated to ultra-high energies. In such a scenario, neutrinos would arise from UHECR interactions in the BBH merger environment. While such a scenario would make BBH mergers promising candidate sources of neutrinos, it is nonetheless worth noting that it remains, as yet, unclear whether sufficiently substantive quantities of material are present at the time of the BBH merger in order to provide an environment for accelerating particles or even to emit electromagnetic radiation and that there have been no definitive reports of detection of electromagnetic counterparts to BBH mergers [167]. As such, we acknowledge that the models that predict neutrino emission from BBH mergers are highly speculative.

For the purposes of predicting the capability of POEMMA for detecting neutrinos from BBH mergers, we use the neutrino flux suggested by Kotera and Silk [20]. In deriving the neutrino flux, they estimated the Poynting flux that can be generated by stellar BHs and, in calculating the maximum neutrino flux, they assumed the Poynting flux can be entirely tapped into UHECRs. The Kotera and Silk neutrino flux includes a parameter, f_ν , for the optical depth to neutrino production. To compute the absolute maximum values for the neutrino flux, we set f_ν equal to one; hence, for this model, the number of neutrino events presented in Table III should be regarded as upper limits. In order to calculate the neutrino fluence, we adopted the time scales of 10^4 s and $10^{6.7}$ s provided in Ref. [168]. Longer time scales lead to more optimistic values for the number of events with tens of events expected from nearby events with the shorter time scales and tens of thousands of events with the longer timescales. For the neutrino horizon, we expect POEMMA to be able to detect neutrinos from BBH mergers out to tens of Mpc for the shorter time scales and out to hundreds of Mpc for the longer time scales. Based on these horizons and the BBH merger event rate measured by LIGO/Virgo of $\mathcal{R} \sim 56_{-27}^{+44} \text{ Gpc}^{-3} \text{ yr}^{-1}$ [150], we expect ~ 10 – 35 BBH merger ToOs per year with POEMMA for the longer time scales. For the shorter time scales, observation times of more than 25 years would be required for one BBH merger ToO event.

2. Other Detectable Transient Source Classes

— *Non-jetted Tidal Disruption Events* — In addition to launching relativistic jets, accretion processes in TDEs can also give rise to AGN-like winds [169–171] and/or colliding tidal streams [172, 173] that could also provide the conditions (*i.e.*, shocks, magnetic reconnection) for accelerating protons and nuclei [17, 174] that would produce neutrinos. In these scenarios, neutrinos from non-jetted and/or misaligned jetted TDEs could be detectable [17]. As such, we include estimates for the numbers of neutrino events and neutrino horizons for these scenarios in Table III. To that end, we adopt the model of Dai and Fang [17] for neutrino production in non-jetted and misaligned TDEs.

In Ref. [17], Dai and Fang modeled TDE neutrino fluences using parameters motivated by observations of nearby bright TDEs and allowing for the possibility of neutrino production outside of a relativistic jet. As such, we adopt these models for calculating the expected number of neutrino events and neutrino horizons from non-jetted and misaligned TDEs. In modeling the neutrino fluence, Dai and Fang determined the total energy injected into cosmic rays over the duration of the TDE (\mathcal{E}_{CR}) that would produce neutrinos. To that end, they adopted two approaches: one in which $\mathcal{E}_{\text{CR}} \sim 10^{51}$ ergs and is presumed the same for every TDE, and one in which \mathcal{E}_{CR} is taken to be ten times the energy emitted in photons as determined from the observed X-ray or optical luminosity of nearby TDEs and a blackbody spectrum. It is worth noting that the value of 10^{51} ergs for the first approach is specifically the value required to produce the neutrino flux measured by IceCube [175] assuming a cosmological rate of $\mathcal{R} \sim 10^{-7} \text{ Mpc}^{-3} \text{ yr}^{-1}$ ⁴, whereas values adopted in the second approach were calculated from observations and assuming that the pion production efficiency $f_\pi \sim 0.1$, leading to lower values for \mathcal{E}_{CR} . Thus, the Dai and Fang [17] calculations of IceCube neutrino events result in higher numbers of events in the first scenario than in the second. For our calculations, we adopt the value of $\mathcal{E}_{\text{CR}} \sim 10^{51}$ ergs for the first model (labelled “average” in Table III). In the second model (labelled “bright” in Table III), we adopt a similar approach to the second scenario presented by Dai and Fang, taking $\mathcal{E}_{\text{CR}} \sim 10 \times E_{\text{rad}}^{\text{obs}} = 5 \times 10^{50}$ ergs (where the value for $E_{\text{rad}}^{\text{obs}}$ was adopted from values provided by Dai and Fang for nearby bright TDEs) but we take

⁴ This rate was calculated in Ref. [17] assuming an observed TDE rate of $\mathcal{R}_{\text{obs}} \sim 10^{-5}$ per galaxy per year [176].

$f_\pi \sim 1$ since f_π in non-jetted scenarios could be substantially different from 0.1 [17]. As such, our calculations for the second model are somewhat more optimistic than for the first model. In either scenario, our calculated neutrino horizons ($z_{\text{hor}} \sim 2.6$ and 5.9 Mpc, respectively, for the “average” and “bright” scenarios) indicate that these events would have to be fairly nearby in order for POEMMA to detect neutrinos. Assuming the Dai and Fang cosmological rate of $\mathcal{R} \sim 10^{-7} \text{ Mpc}^{-3} \text{ yr}^{-1}$, POEMMA would have to be observing for substantially longer than 25 years in order to observe one such event. Higher rates suggested by some references in the literature [see *e.g.*, 177] or by the upper limit of the Lunardini and Winter [18] rate (after correcting for the jet solid angle) would imply higher ToO rates, but still at the level of $\lesssim 1$ per 25-year observation.

— *Gamma-ray Bursts* — GRBs are associated with the deaths of massive stars and/or the birth of stellar-mass compact objects. The population of GRBs can be divided into two categories: long duration GRBs (LGRBs) with gamma-ray light curves lasting more than 2 seconds, and short duration GRBs (sGRBs) with gamma-ray light curves that are shorter than 2 seconds. LGRBs have been linked with core-collapse supernovae of massive stars ($\gtrsim 25M_\odot$, whereas sGRBs are thought to arise from the merger of two neutron stars or the merger of a neutron star with a black hole. In either scenario, the phenomenology of GRBs can be described through the framework of the fireball model [178–181]. In this model, the creation of a compact object results in the release of a large quantity of gravitational energy of which some portion is released in the form of an optically thick fireball of high-energy radiation and particles funneled into a relativistic jet that plows through the circumburst and interstellar environment giving rise to the complex observational phenomenology associated with GRBs. Similar to the source classes that have already been discussed in this paper, the conditions that are expected to be present in GRB jets could allow for the acceleration of UHECRs and the associated production of neutrinos (*i.e.*, strong shocks and magnetic fields that would allow for shock acceleration, turbulent plasma that are conducive to magnetic reconnection, and similar phenomena). The pioneering works of Waxman in Ref. [182] and Waxman and Bahcall in Ref. [14] set the stage for extensive work in the literature on the topic of UHECR and neutrinos from GRBs [see *e.g.*, 15, 16, 113, 138, 183–192; for detailed review and more complete reference list see 193].

As noted earlier, BNS mergers provide conditions for accelerating UHECRs. In contrast to the process discussed earlier in which neutrinos are produced by UHECRs accelerated in the magnetosphere of a

stable massive neutron star resulting from the BNS merger, we now explore neutrinos produced in the sGRB that would occur during or immediately following the BNS merger. In Ref. [16], KMMK modeled neutrino fluences from various phases of sGRBs, including the prompt phase and the extended emission phase accompanying $\sim 25\%$ of sGRBs [194], for various assumptions for key GRB jet parameters. In Ref. [61], the ANTARES, IceCube, and Pierre Auger Collaborations compared their sensitivities to KMMK modeled fluences rescaled to a luminosity distance of 40 Mpc. For sGRBs that are viewed on-axis, IceCube can constrain scenarios with more optimistic neutrino fluences as long as the source is within ~ 40 Mpc. At the higher energies where Auger has sensitivity, the predicted neutrino fluences are substantially lower and would be undetectable for a source at 40 Mpc in the case of neutrino emission from the extended emission phase. Predicted neutrino fluences from other phases of the sGRBs are even lower, implying that the source would have to be on the order of a factor of two (for an X-ray flare neutrinos) up to a factor of six (for prompt phase neutrinos) closer to be detectable by Auger. In order to assess the capability of POEMMA to detect neutrinos from the various phases of sGRBs, we perform calculations for the moderate extended emission and the prompt phase models of KMMK. For sources located on the order of a few Mpc, we expect POEMMA to detect on the order of hundreds to thousands of neutrinos in the case of neutrinos from the extended emission phase and on the order of tens of neutrinos from the prompt phase. We calculate that the neutrino horizons for POEMMA are on the order of 120 Mpc for extended emission model and on the order of 30 Mpc for the prompt phase model. Taking the local sGRB rate of $4\text{--}10 \text{ Gpc}^{-3} \text{ yr}^{-1}$ [195] and multiplying by a factor of 0.25 for the extended emission model (as only 25% of sGRBs have extended emission), we find that these horizon imply ToO rates of $\lesssim 1$ per 25-year observation period with POEMMA, with much higher rates in the case of neutrinos from extended emission phase than in the case of neutrinos from the prompt phase owing to the much higher neutrino fluences in the extended emission model.

We also consider the possibility of detecting neutrinos from LGRBs. As in the case of sGRBs, neutrino production has been studied in all of the various phases of LGRBs. For our calculations for the sensitivity of POEMMA to LGRBs, we adopt models from Ref. [15]. Both models consider neutrino production in the LGRB early afterglow, *i.e.*, the point at which the expanding fireball strikes the surrounding medium. At this point, two shocks are formed: a forward shock that continues to propagate into

the surrounding medium, and a reverse shock that propagates back into the ejecta. In the two models considered from Ref. [15], neutrino production in the early afterglow arises from UHECR acceleration by the reverse shock.⁵ Given the uncertainty in the circumburst environment, Murase considered two types of environments: a homogeneous environment suggestive of the interstellar medium (ISM), and a parametrized model that simulated an environment that would have included material that had been blown off of the massive progenitor star over the course of its lifetime (wind). Target photons from the early afterglow and the overlapping prompt emission were included in the models. For this paper, we considered ISM and wind early-afterglow models that also included the effect of the overlapping prompt emission. Late prompt neutrino models that were also studied by Murase yield results that are similar to those for the wind model provided in Table III. As the wind model predicts higher neutrino fluences than the ISM model by roughly two orders of magnitudes, the results in the wind scenario are quite a bit more optimistic. An LGRB resembling the ISM model would have to be within 3 Mpc in order to be detectable by POEMMA. On the other hand, for an LGRB resembling the wind model, we expect that POEMMA will be able to detect tens to hundreds of neutrinos for sources at distances on the order of a few Mpc. In this model, POEMMA will be able to detect neutrinos out to a distance of on the order of 40 Mpc. Based on the local LGRB rate of $0.42 \text{ Gpc}^{-3} \text{ yr}^{-1}$ [196], we expect a ToO rate of $\lesssim 1$ per 25-year observation period with POEMMA.

— *Newly-born Pulsars and Magnetars from Core-Collapse Supernovae* — As noted earlier, newly born, rapidly spinning magnetars are promising candidate sources of UHECRs and neutrinos depending on the nature of the environment of the magnetar. The surrounding medium of a pulsar and a magnetar formed in a core-collapse supernova is likely to be distinct from that resulting from a BNS merger as the environment in the former is characteristic of stellar material from the exploding star whereas the environment of the latter would be characteristic of tidal debris from the merging neutron stars and the associated radiation [146]. In fact, CRs accelerated by core-collapse pulsars and magnetars will readily interact in the surrounding medium, preventing their escape as UHECRs; on the other hand, these interactions will produce high-energy neutri-

nos [23, 197, 198]. In Ref. [23], Fang modeled neutrino production by newly-born core-collapse pulsars and magnetars under various assumptions for the magnetic field strength, spin period, and CR composition. In evaluating the sensitivity of POEMMA to detect neutrinos from these sources, we adopt three models from Ref. [23]: a Crab-like pulsar model with pure proton composition, a magnetar model with pure proton composition, and a magnetar model with pure iron composition. In the Crab-like model, the lower magnetic fields and longer spin period limits the energy of the accelerated CRs, and very few of them are accelerated to ultra-high energies. As such, the neutrino fluence arising from Crab-like pulsars is expected to be very low; in fact, we find that such a source would have to be inside or very close to the Galaxy in order to be detectable by POEMMA. In contrast, the magnetar models result in higher neutrino fluences as more CRs are accelerated to ultra-high energies in these models. Our results for these two models are roughly similar, though the pure iron model results in slightly more neutrino events since the maximum energy for iron is 26 times that of protons. For these models, we expect POEMMA to detect tens of thousands of neutrinos from a newly-born magnetar at the GC. The horizons for these models are on the order of 1–2 Mpc, indicating that the magnetar would have to be fairly close to be detectable by POEMMA. In order to estimate the expected ToO rate, we use the local rate of superluminous supernovae expected to produce magnetars provided by Refs. [199, 200], $\mathcal{R} \sim 21 \text{ Gpc}^{-3} \text{ yr}^{-1}$. Based on this rate, we expect a ToO rate of $\ll 1$ per 25-year observation time with POEMMA. The rate for less luminous supernovae is many orders of magnitude higher: $\mathcal{R} \simeq (1.06 \pm 0.19) \times 10^{-4} \text{ Mpc}^{-3} \text{ yr}^{-1}$ [201]; however, the much smaller horizon for Crab-like pulsars implies a ToO rate that is comparable to those of the magnetar models considered here.

— *Binary White Dwarf Mergers* — In addition to BNS merger events and core-collapse supernovae, rapidly spinning magnetars can be produced by binary white dwarf (BWD) mergers, making such mergers promising events for UHECR production [202]. Small amounts of surrounding material ($\sim 0.1 M_{\odot}$) allows UHECRs to escape the system more easily than in magnetars formed in core-collapse supernovae [202]; on the other hand, the limited amount of surrounding material leads to lower neutrino fluxes [202]. Alternatively, the magnetorotational instability that can develop in the debris disk surrounding the magnetar can lead to the formation of a hot, magnetized corona and high-velocity outflows [22, 203–205]. Magnetic reconnection can accelerate cosmic rays that would interact with outflow material and radiation to pro-

⁵ Murase argues that neutrino production is negligible in the forward shock as the maximum energy for CRs accelerated in the forward shock is on the order of a few PeV [15].

duce high-energy neutrinos as modeled by Xiao et al. (XMMD) in Ref. [22]. We adopt the XMMD model to determine the sensitivity of POEMMA to neutrinos from BWD mergers. The modeled neutrino fluences are very low – for an event that occurs at the GC, we expect POEMMA to detect on the order of 20 neutrinos, which is a substantially lower number than predicted by any of the other models. In fact, in order for POEMMA to detect neutrinos from these events, the source would have to be within the Galaxy. Based on an event rate provided in Ref. [22] (see also Ref. [206]), which is comparable to the Type Ia supernova rate, we expect a ToO rate that is $\ll 1$ per 25-year observation time with POEMMA.

IV. CONCLUSIONS

While at any particular time only transient sources below the limb of the Earth as viewed from the satellites are relevant to tau neutrino induced upward-going air shower signals, POEMMA and other space-based instruments will have full-sky coverage over the orbital period of the satellites and the precession period of the orbital plane. The slewing capability of POEMMA in time frames of on the order of 500 s will permit target of opportunity observations identified via electromagnetic or gravitational messenger. In some cases, POEMMA observations may signal an alert.

Measurements of the diffuse flux of neutrinos from space will benefit only slightly in lower-energy sensitivity by extending the viewing band further back from the limb [56]. For the diffuse flux, the standard configuration has neutrino viewing to 7° below the horizon. For target of opportunity events, a broader angular range will be accessible to POEMMA before neutrino flux attenuation in the Earth obscures a neutrino source. Our results here are based on tau elevation angles $\beta_{\text{tr}} > 35^\circ$, equivalent to viewing from the satellites to an angle of $\sim 20^\circ$ below the limb. The capability for tracking the source means that the best case sensitivities for POEMMA are as much as two orders of magnitude better than those of Auger as reported in Ref. [61] with all-sky coverage. Based on the calculations performed here, we predict that POEMMA will be able to observe TDEs, blazar flares, BBH mergers, and BNS mergers within a 25-year observation period.

Long bursts within luminosity distances specified in Table III will be observable by POEMMA, regardless of location. For short duration bursts, the sensitivity will be better than for long bursts if the source is well placed relative to the Earth and POEMMA. However, short bursts may not be observable if the source does not dip below the Earth’s horizon, or if

the burst occurs when the Sun and/or Moon interfere with observing.

Sources described here, with associated numbers of events, follow from standard model (SM) processes. The ANITA Collaboration has reported two unusual events, which qualitatively look like air showers initiated by energetic (~ 500 PeV) particles that emerge from the ice along trajectories with large elevation angles [207, 208]. However, at these high energies neutrinos are expected to interact inside Earth with a high probability. For the angles inferred from ANITA observations, the ice would be well screened from up-going neutrinos by the underlying layers of Earth, challenging SM explanations [209, 210]. Several beyond SM physics models have been proposed to explain ANITA events [211–221], but systematic effects of data analysis cannot be discarded yet [222, 223]. POEMMA will have detection capabilities for such events. For example, a 600 PeV EAS will yield a signal of more than 10,000 photons/m² for 35° Earth-emergence angle, meaning a photoelectron signal that is a factor of 500 times greater than the 10 PE threshold. Relative to ANITA, POEMMA will have a factor of ~ 10 increase in acceptance solid angle since these EASs are so bright. POEMMA, in tracking neutrino sources, will also be sensitive to non-standard model particles that generate up-going EASs.

Acknowledgements

We would like to thank Roopesh Ojha and Elizabeth Hays for helpful discussions about AGNs and ToOs. We would also like to thank our colleagues of the Pierre Auger and POEMMA collaborations for valuable discussions. This work is supported in part by US Department of Energy grant DE-SC-0010113, NASA grant 17-APRA17-0066, NASA awards NNX17AJ82G and 80NSSC18K0464, and the U.S. National Science Foundation (NSF Grant PHY-1620661).

Appendix A: POEMMA detection for $\beta_{\text{tr}} < 35^\circ$

Many of the details required for the evaluation of the POEMMA effective area follow from the discussion of the sensitivity to the diffuse flux in Ref. [56]. Figure 11 shows the configuration of POEMMA at altitude $h = 525$ km and a tau emerging at a local zenith angle θ_{tr} . In practice, we consider angles θ_{tr} close ($\lesssim \theta_{\text{Ch}}^{\text{eff}} \sim 1.5^\circ$) to the local zenith angle θ_v of the line of sight as required for detection of the showers. The difference in angles θ_{tr} and θ_v in Fig. 11 is

exaggerated for clarity.

For tau air showers, it is common to use the local elevation angle to describe the trajectory rather than the local zenith angle. The elevation angles, labeled with β , are defined by angles relative to the local tangent plane, e.g., $\beta_{\text{tr}} = 90^\circ - \theta_{\text{tr}}$.

The tau decay at a distance s is viewable for decays within a cone of opening angle $\theta_{\text{Ch}}^{\text{eff}}$. The effective area for the tau air shower that begins s from the point of emergence on the Earth is shown by the dashed disk on the figure. The area of the disk is expressed in Eq. (1).

For the ToO neutrino sources, the slewing capabilities of POEMMA allow for a larger range of viewing below the limb, or alternatively, a larger range of elevation angles β_{tr} .

We show the tau exit probability for angles up to $\beta_{\text{tr}} = 35^\circ$ in Fig. 12. Neutrino attenuation becomes increasing important for larger β_{tr} and higher neutrino energies. Tau neutrino regeneration is included here, namely, multiple iterations of $\nu_\tau \rightarrow \tau$ production for weak scattering with nucleons, and $\tau \rightarrow \nu_\tau$ regeneration through decays.

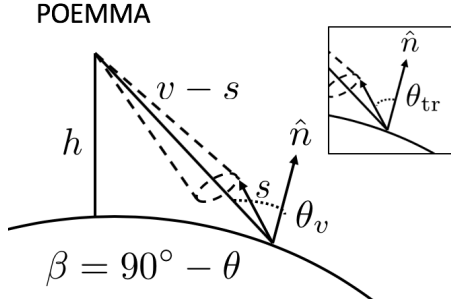


FIG. 11. The effective area (dashed disk on the figure) for a tau air shower that begins a path length s from the point of emergence on the Earth. The local zenith angle of the line of sight, of distance v , is θ_v . The inset shows the emergence angle of the tau θ_{tr} .

Figures 13 and 14 are EAS parameter inputs to the detection probability calculated by a neutrino sensitivity Monte Carlo. They are derived from modeling of the upward EAS development, Cherenkov signal generation, and atmospheric attenuation of the Cherenkov signal (see Ref. [56]). The EAS development is modeled using shower-universality and provides an average EAS profile for a given energy and Earth-emergence angle (β_{tr}), with the assumption that 50% of the tau's energy goes into the EAS. The Cherenkov angle is calculated from the modeling as a function of altitude and β_{tr} , which is sampled in the POEMMA neutrino sensitivity Monte Carlo. The Cherenkov angle variations shown in Fig. 13 are mainly due to the fact that the atmosphere density decreases as function of alti-

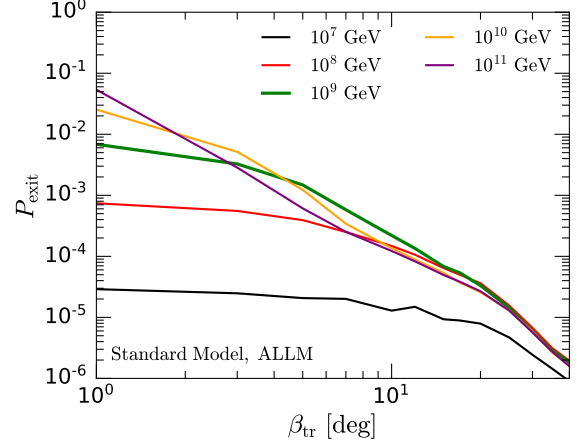


FIG. 12. The exit probability for a ν_τ of a given energy to emerge as a τ -lepton as a function of elevation angle β_{tr} .

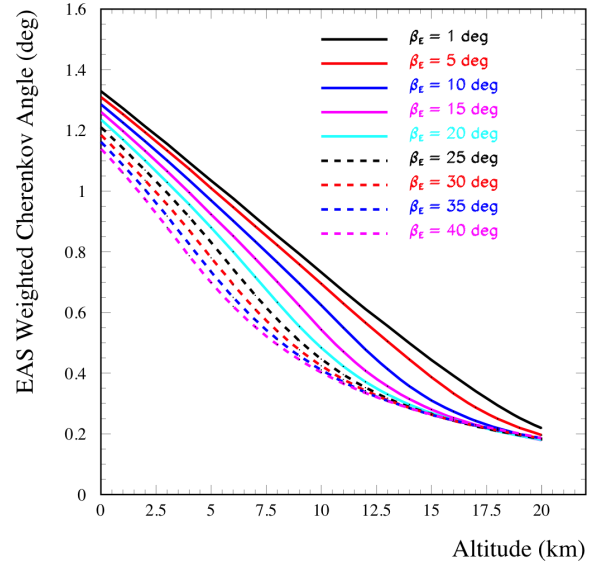


FIG. 13. The effective Cherenkov angle of the air shower as a function of altitude of the tau decay and elevation angle β_{tr} for an upward-moving 100 PeV EAS.

tude, e.g., the index of refraction of air decreases as altitude increases, with an additional effect because EAS development at larger β_{tr} spans larger ranges of altitudes. The Cherenkov photon yield, shown in Fig. 14 for 100 PeV EASs is more complicated. This is best illustrated by examining the variation in photon yield for EASs starting at sea level as a function of β_{tr} . At the lowest altitudes, the Cherenkov light attenuation is dominated by aerosol scattering due to the aerosol distribution having a scale height of ~ 1 km. As β_{tr} increases, a larger fraction of the EAS development occurs at higher altitudes where the aerosol contribution becomes smaller, thus lead-

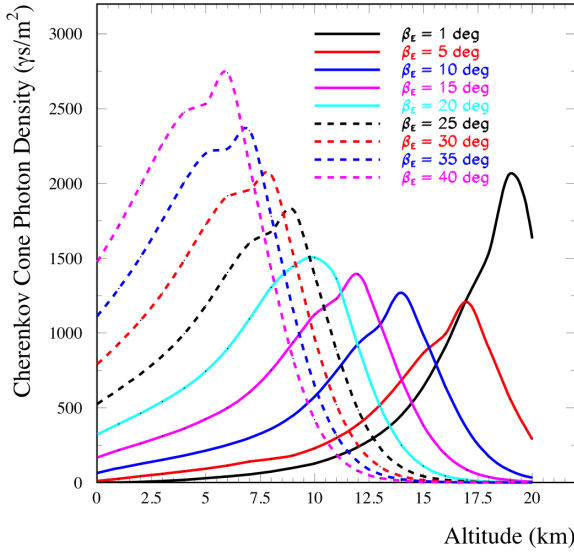


FIG. 14. The photon density at POEMMA a function of altitude of the tau decay and elevation angle β_{tr} for 100 PeV upward-moving EAS.

ing to a larger Cherenkov photon density at 525 km. This effectively leads to a lower energy threshold for tau-induced EAS detection for larger β_{tr} . In regards to the altitude variation, for a given E, β_{tr} there is an altitude where the atmosphere becomes too rarefied to support EAS development. This leads to the turn over of the photon densities at higher altitudes shown in Fig. 14. Note that the neutrino sensitivity Monte Carlo effectively uses the results shown in Figs. 13 and 14 to generate the EAS signals for a specific tau decay by interpolating the Cherenkov angle and photon density results to obtain those for a given tau EAS geometry, with linearly scaling as a function of shower energy for the photon yield.

Appendix B: Cosmological Fluences

For $\Omega_k = 0$, the comoving transverse distance d_M is equivalent to the line-of-sight comoving distance

$$d_C = \frac{c}{H_0} \int_0^z \frac{dz'}{E(z')}, \quad (B1)$$

i.e., $d_C = d_M$ [73]. The luminosity distance d_L is defined by the relationship between bolometric (i.e., integrated over all frequencies) energy-flux S and bolometric luminosity L :

$$d_L = \sqrt{\frac{L}{4\pi S}}. \quad (B2)$$

Now, using (14) it is straightforward to see that

$$d_L = (1+z)d_M. \quad (B3)$$

While sources often do not emit isotropically, we consider fluences based on *isotropic equivalent* quantities. With this in mind, the total neutrino fluence at a line-of-sight distance d_M can be written as

$$\phi_\nu(E_\nu) = \frac{d^2 N_\nu}{dE_\nu dA_{\text{sph}}}, \quad (B4)$$

where A_{sph} is the spherical area of radius d_M . The number of neutrinos crossing the area A_{sph} is then given by

$$N_\nu = 4\pi d_M^2 \phi_\nu(E_\nu) \Delta E_\nu. \quad (B5)$$

On the other hand, the number of emitted neutrinos in a time interval Δt_{src} is found to be

$$N_{\text{src}} = Q(E_{\text{src}}) \Delta t_{\text{src}} \Delta E_{\text{src}}, \quad (B6)$$

where $Q(E_{\text{src}})$ is the (all flavor) neutrino source emission rate and E_{src} indicates the emission energy. Setting the number of neutrinos distributed over the sphere of area A_{sph} equal to the number of emitted neutrinos and re-arranging to isolate the fluence at the observation distance d_M , we obtain

$$\phi_\nu = \left(\frac{1}{4\pi d_M^2} \right) Q(E_{\text{src}}) \Delta t_{\text{src}} \frac{\Delta E_{\text{src}}}{\Delta E_\nu}. \quad (B7)$$

Accounting for the redshift z , the energy scales as $E_{\text{src}} = (1+z)E_\nu$, and therefore the energy-squared scaled fluence at the observation point is

$$E_\nu^2 \phi_\nu = \frac{(1+z)}{4\pi d_L^2} E_{\text{src}}^2 Q(E_{\text{src}}) \Delta t_{\text{src}}. \quad (B8)$$

Finally, dividing Eq. (B8) by 3 to account for the fact that only 1/3 of the emitted neutrinos are of tau flavor we obtain the desired result displayed in Eq. (18). As such, for any model that provides an observed fluence and a source redshift or luminosity distance, one can determine $E_{\text{src}}^2 Q(E_{\text{src}}) \Delta t_{\text{src}}$. We use Eq. (18) to calculate the observed single-flavor neutrino fluence at *any* redshift z . The maximum redshift at which we can see the event, z_{hor} , is the redshift at which N_{ev} in Eq. (17) is equal to 1.0.

-
- [1] **LIGO Scientific, Virgo Collaboration**, B. P. Abbott *et al.*, “GW170817: Observation of Gravitational Waves from a Binary Neutron Star Inspiral,” *Phys. Rev. Lett.* **119** no. 16, (2017) 161101, [arXiv:1710.05832 \[gr-qc\]](#). I, II B 1
- [2] **LIGO Scientific, Virgo, Fermi GBM, INTEGRAL, IceCube, AstroSat Cadmium Zinc Telluride Imager Team, IPN, Insight-Hxmt, ANTARES, Swift, AGILE Team, 1M2H Team, Dark Energy Camera GW-EM, DES, DLT40, GRAWITA, Fermi-LAT, ATCA, ASKAP, Las Cumbres Observatory Group, OzGrav, DWF (Deeper Wider Faster Program), AST3, CAASTRO, VINROUGE, MASTER, J-GEM, GROWTH, JAGWAR, CaltechNRAO, TTU-NRAO, NuSTAR, Pan-STARRS, MAXI Team, TZAC Consortium, KU, Nordic Optical Telescope, ePESSTO, GROND, Texas Tech University, SALT Group, TOROS, BOOTES, MWA, CALET, IKI-GW Follow-up, H.E.S.S., LOFAR, LWA, HAWC, Pierre Auger, ALMA, Euro VLBI Team, Pi of Sky, Chandra Team at McGill University, DFN, ATLAS Telescopes, High Time Resolution Universe Survey, RIMAS, RATIR, SKA South Africa/MeerKAT Collaboration**, B. P. Abbott *et al.*, “Multi-messenger Observations of a Binary Neutron Star Merger,” *Astrophys. J.* **848** no. 2, (2017) L12, [arXiv:1710.05833 \[astro-ph.HE\]](#). I
- [3] **IceCube, Fermi-LAT, MAGIC, AGILE, ASAS-SN, HAWC, H.E.S.S., INTEGRAL, Kanata, Kiso, Kapteyn, Liverpool Telescope, Subaru, Swift NuSTAR, VERITAS, VLA/17B-403 Collaboration**, M. G. Aartsen *et al.*, “Multimessenger observations of a flaring blazar coincident with high-energy neutrino IceCube-170922A,” *Science* **361** no. 6398, (2018) eaat1378, [arXiv:1807.08816 \[astro-ph.HE\]](#). I, 3, II B 1
- [4] **Pierre Auger Collaboration**, A. Aab *et al.*, “Improved limit to the diffuse flux of ultrahigh energy neutrinos from the Pierre Auger Observatory,” *Phys. Rev.* **D91** no. 9, (2015) 092008, [arXiv:1504.05397 \[astro-ph.HE\]](#). I
- [5] **Pierre Auger Collaboration**, A. Aab *et al.*, “Ultrahigh-Energy Neutrino Follow-Up of Gravitational Wave Events GW150914 and GW151226 with the Pierre Auger Observatory,” *Phys. Rev.* **D94** no. 12, (2016) 122007, [arXiv:1608.07378 \[astro-ph.HE\]](#).
- [6] **Telescope Array Collaboration**, R. U. Abbasi *et al.*, “Search for Ultra-High-Energy Neutrinos with the Telescope Array Surface Detector,” [arXiv:1905.03738 \[astro-ph.HE\]](#).
- [7] **ARIANNA Collaboration**, A. Anker *et al.*, “Targeting cosmogenic neutrinos with the ARIANNA experiment,” [arXiv:1903.01609 \[astro-ph.IM\]](#).
- [8] **IceCube Collaboration**, M. G. Aartsen *et al.*, “Differential limit on the extremely-high-energy cosmic neutrino flux in the presence of astrophysical background from nine years of IceCube data,” *Phys. Rev.* **D98** no. 6, (2018) 062003, [arXiv:1807.01820 \[astro-ph.HE\]](#).
- [9] **MAGIC Collaboration**, M. L. Ahnen *et al.*, “Limits on the flux of tau neutrinos from 1 PeV to 3 EeV with the MAGIC telescopes,” *Astropart. Phys.* **102** (2018) 77–88, [arXiv:1805.02750 \[astro-ph.IM\]](#).
- [10] **ARA Collaboration**, P. Allison *et al.*, “Performance of two Askaryan Radio Array stations and first results in the search for ultrahigh energy neutrinos,” *Phys. Rev.* **D93** no. 8, (2016) 082003, [arXiv:1507.08991 \[astro-ph.HE\]](#).
- [11] **Pierre Auger Collaboration**, A. Aab *et al.*, “Multi-Messenger Physics with the Pierre Auger Observatory,” *Front. Astron. Space Sci.* **6** (2019) 24, [arXiv:1904.11918 \[astro-ph.HE\]](#). I
- [12] P. Meszaros, “Astrophysical Sources of High Energy Neutrinos in the IceCube Era,” *Ann. Rev. Nucl. Part. Sci.* **67** (2017) 45–67, [arXiv:1708.03577 \[astro-ph.HE\]](#). I
- [13] M. Ackermann *et al.*, “Astrophysics Uniquely Enabled by Observations of High-Energy Cosmic Neutrinos,” [arXiv:1903.04334 \[astro-ph.HE\]](#). I
- [14] E. Waxman and J. N. Bahcall, “High-energy neutrinos from cosmological gamma-ray burst fireballs,” *Phys. Rev. Lett.* **78** (1997) 2292–2295, [arXiv:astro-ph/9701231 \[astro-ph\]](#). I, II B 1, II B 2
- [15] K. Murase, “High energy neutrino early afterglows gamma-ray bursts revisited,” *Phys. Rev.* **D76** (2007) 123001, [arXiv:0707.1140 \[astro-ph\]](#). III, II B 2, II B 2, II B 2, 5
- [16] S. S. Kimura, K. Murase, P. Mészáros, and K. Kiuchi, “High-Energy Neutrino Emission from Short Gamma-Ray Bursts: Prospects for Coincident Detection with Gravitational Waves,” *Astrophys. J.* **848** no. 1, (2017) L4, [arXiv:1708.07075 \[astro-ph.HE\]](#). I, 4, III, 10, II B 2, II B 2
- [17] L. Dai and K. Fang, “Can tidal disruption events produce the IceCube neutrinos?,” *Mon. Not. Roy. Astron. Soc.* **469** no. 2, (2017) 1354–1359, [arXiv:1612.00011 \[astro-ph.HE\]](#). I, III, II B 1, II B 2, II B 2, II B 2, II B 2, 4, II B 2
- [18] C. Lunardini and W. Winter, “High Energy Neutrinos from the Tidal Disruption of Stars,” *Phys. Rev.* **D95** no. 12, (2017) 123001, [arXiv:1612.03160 \[astro-ph.HE\]](#). I, III, II B 1, II B 1, II B 1, II B 1, II B 1, II B 1, II B 2
- [19] X. Rodrigues, A. Fedynitch, S. Gao, D. Boncioli, and W. Winter, “Neutrinos and

- Ultra-High-Energy Cosmic-Ray Nuclei from Blazars,” *Astrophys. J.* **854** no. 1, (2018) 54, [arXiv:1711.02091 \[astro-ph.HE\]](#). I, II, 2, III, IIIB 1, IIIB 1, 10
- [20] K. Kotera and J. Silk, “Ultrahigh Energy Cosmic Rays and Black Hole Mergers,” *Astrophys. J.* **823** no. 2, (2016) L29, [arXiv:1602.06961 \[astro-ph.HE\]](#). I, III, IIIB 1, IIIB 1
- [21] K. Fang and B. D. Metzger, “High-Energy Neutrinos from Millisecond Magnetars formed from the Merger of Binary Neutron Stars,” *Astrophys. J.* **849** no. 2, (2017) 153, [arXiv:1707.04263 \[astro-ph.HE\]](#). [Astrophys. J.849,153(2017)]. I, II, 2, III, 10, IIIB 1, IIIB 1
- [22] D. Xiao, P. Mészáros, K. Murase, and Z.-g. Dai, “High-Energy Neutrino Emission from White Dwarf Mergers,” *Astrophys. J.* **832** no. 1, (2016) 20, [arXiv:1608.08150 \[astro-ph.HE\]](#). I, III, IIIB 2, IIIB 2, IIIB 2
- [23] K. Fang, “High-Energy Neutrino Signatures of Newborn Pulsars In the Local Universe,” *JCAP* **1506** no. 06, (2015) 004, [arXiv:1411.2174 \[astro-ph.HE\]](#). I, III, IIIB 2, IIIB 2, IIIB 2
- [24] R. Gandhi, C. Quigg, M. H. Reno, and I. Sarcevic, “Neutrino interactions at ultrahigh-energies,” *Phys. Rev.* **D58** (1998) 093009, [arXiv:hep-ph/9807264 \[hep-ph\]](#). I
- [25] P. Lipari, M. Lusignoli, and D. Meloni, “Flavor Composition and Energy Spectrum of Astrophysical Neutrinos,” *Phys. Rev.* **D75** (2007) 123005, [arXiv:0704.0718 \[astro-ph\]](#). I
- [26] **Particle Data Group** Collaboration, M. Tanabashi *et al.*, “Review of Particle Physics,” *Phys. Rev.* **D98** no. 3, (2018) 030001. I
- [27] J. G. Learned and S. Pakvasa, “Detecting tau-neutrino oscillations at PeV energies,” *Astropart. Phys.* **3** (1995) 267–274, [arXiv:hep-ph/9405296 \[hep-ph\]](#). I
- [28] G. Domokos and S. Kovesi-Domokos, “Observation of UHE interactions neutrinos from outer space,” [arXiv:hep-ph/9801362 \[hep-ph\]](#). [AIP Conf. Proc.433,390(1998)]. I
- [29] D. Fargion, “Discovering Ultra High Energy Neutrinos by Horizontal and Upward tau Air-Showers: Evidences in Terrestrial Gamma Flashes?,” *Astrophys. J.* **570** (2002) 909–925, [arXiv:astro-ph/0002453 \[astro-ph\]](#).
- [30] D. Fargion, “Tau neutrino astronomy,” in *Beyond the desert. Proceedings, 4th International Conference, Particle physics beyond the standard model, BEYOND 2003, Castle Ringberg, Tegernsee, Germany, June 9-14, 2003*, pp. 831–856. 2003.
- [31] D. Fargion, P. De Sanctis Lucentini, and M. De Santis, “Tau air showers from earth,” *Astrophys. J.* **613** (2004) 1285–1301, [arXiv:hep-ph/0305128 \[hep-ph\]](#).
- [32] S. Palomares-Ruiz, A. Irimia, and T. J. Weiler, “Acceptances for space-based and ground-based fluorescence detectors, and inference of the neutrino-nucleon cross-section above 10^{19} -ev,” *Phys. Rev.* **D73** (2006) 083003, [arXiv:astro-ph/0512231 \[astro-ph\]](#).
- [33] A. Neronov, D. V. Semikoz, L. A. Anchordoqui, J. Adams, and A. V. Olinto, “Sensitivity of a proposed space-based Cherenkov astrophysical-neutrino telescope,” *Phys. Rev.* **D95** no. 2, (2017) 023004, [arXiv:1606.03629 \[astro-ph.IM\]](#).
- [34] A. V. Olinto *et al.*, “POEMMA: Probe Of Extreme Multi-Messenger Astrophysics,” *PoS ICRC2017* (2018) 542, [arXiv:1708.07599 \[astro-ph.IM\]](#). [35,542(2017)]. I
- [35] A. V. Olinto, “POEMMA and EUSO-SPB: Space Probes of the Highest Energy Particles,” in *Proceedings, Vulcano Workshop 2018: Frontier Objects in Astrophysics and Particle Physics: Vulcano Island, Sicily, Italy, May 20-26, 2018*, pp. 370–385. 2018.
- [36] **ANITA** Collaboration, P. W. Gorham *et al.*, “Constraints on the diffuse high-energy neutrino flux from the third flight of ANITA,” *Phys. Rev.* **D98** no. 2, (2018) 022001, [arXiv:1803.02719 \[astro-ph.HE\]](#).
- [37] **ANITA** Collaboration, P. W. Gorham *et al.*, “Constraints on the ultra-high energy cosmic neutrino flux from the fourth flight of ANITA,” [arXiv:1902.04005 \[astro-ph.HE\]](#).
- [38] **OWL** Collaboration, J. F. Krizmanic, J. W. Mitchell, and R. E. Streitmatter, “Optimization of the Orbiting Wide-angle Light Collectors (OWL) Mission for Charged-Particle and Neutrino Astronomy,” in *Proceedings, 33rd International Cosmic Ray Conference (ICRC2013): Rio de Janeiro, Brazil, July 2-9, 2013*, p. 1085. 2013. [arXiv:1307.3907 \[astro-ph.IM\]](#). I
- [39] X. Bertou, P. Billoir, O. Deligny, C. Lachaud, and A. Letessier-Selvon, “Tau neutrinos in the Auger Observatory: A New window to UHECR sources,” *Astropart. Phys.* **17** (2002) 183–193, [arXiv:astro-ph/0104452 \[astro-ph\]](#). I
- [40] J. L. Feng, P. Fisher, F. Wilczek, and T. M. Yu, “Observability of earth skimming ultrahigh-energy neutrinos,” *Phys. Rev. Lett.* **88** (2002) 161102, [arXiv:hep-ph/0105067 \[hep-ph\]](#).
- [41] C. Lachaud, X. Bertou, P. Billoir, O. Deligny, and A. Letessier-Selvon, “Probing the GZK barrier with UHE tau neutrinos,” *Nucl. Phys. Proc. Suppl.* **110** (2002) 525–527.
- [42] C. Aramo, A. Insolia, A. Leonardi, G. Miele, L. Perrone, O. Pisanti, and D. V. Semikoz, “Earth-skimming UHE Tau neutrinos at the fluorescence detector of Pierre Auger observatory,” *Astropart. Phys.* **23** (2005) 65–77, [arXiv:astro-ph/0407638 \[astro-ph\]](#).
- [43] **Pierre Auger** Collaboration, P. Abreu *et al.*, “Search for point-like sources of ultra-high energy neutrinos at the Pierre Auger Observatory and improved limit on the diffuse flux of tau neutrinos,” *Astrophys. J.* **755** (2012) L4,

- [arXiv:1210.3143 \[astro-ph.HE\]](#). I, II
- [44] G. W. Hou and M. Huang, “Expected performance of a neutrino telescope for seeing AGN / GC behind a mountain,” [arXiv:astro-ph/0204145 \[astro-ph\]](#). I
- [45] Y. Asaoka and M. Sasaki, “Cherenkov Tau Shower Earth-Skimming Method for PeV-EeV Tau Neutrino Observation with Ashra,” *Astropart. Phys.* **41** (2013) 7–16, [arXiv:1202.5656 \[astro-ph.HE\]](#).
- [46] A. N. Otte, “Trinity: An Air-Shower Imaging System for the Detection of Cosmogenic Neutrinos,” [arXiv:1811.09287 \[astro-ph.IM\]](#).
- [47] **GRAND** Collaboration, J. Alvarez-Muñiz *et al.*, “The Giant Radio Array for Neutrino Detection (GRAND): Science and Design,” [arXiv:1810.09994 \[astro-ph.HE\]](#).
- [48] A. Neronov, “Sensitivity of top-of-the-mountain fluorescence telescope system for astrophysical neutrino flux above 10 PeV,” [arXiv:1905.10606 \[astro-ph.HE\]](#). I
- [49] F. Halzen and D. Saltzberg, “Tau-neutrino appearance with a 1000 megaparsec baseline,” *Phys. Rev. Lett.* **81** (1998) 4305–4308, [arXiv:hep-ph/9804354 \[hep-ph\]](#). I
- [50] F. Becattini and S. Bottai, “Extreme energy neutrino(tau) propagation through the Earth,” *Astropart. Phys.* **15** (2001) 323–328, [arXiv:astro-ph/0003179 \[astro-ph\]](#).
- [51] S. I. Dutta, M. H. Reno, and I. Sarcevic, “Tau neutrinos underground: Signals of muon-neutrino \rightarrow tau neutrino oscillations with extragalactic neutrinos,” *Phys. Rev.* **D62** (2000) 123001, [arXiv:hep-ph/0005310 \[hep-ph\]](#).
- [52] J. F. Beacom, P. Crotty, and E. W. Kolb, “Enhanced signal of astrophysical tau neutrinos propagating through earth,” *Phys. Rev.* **D66** (2002) 021302, [arXiv:astro-ph/0111482 \[astro-ph\]](#).
- [53] J. Alvarez-Muñiz, W. R. Carvalho, A. L. Cummings, K. Payet, A. Romero-Wolf, H. Schoorlemmer, and E. Zas, “Comprehensive approach to tau-lepton production by high-energy tau neutrinos propagating through the Earth,” *Phys. Rev.* **D97** no. 2, (2018) 023021, [arXiv:1707.00334 \[astro-ph.HE\]](#). [erratum: *Phys. Rev.D99*,no.6,069902(2019)]. I
- [54] A. V. Olinto *et al.*, “Poemina: Probe of extreme multi-messenger astrophysicsMS Windows NT kernel description.” https://smd-prod.s3.amazonaws.com/science-pink/s3fs-public/atoms/files/1_POEMMA_Study_Rpt_0.pdf. Accessed: 2019-05-19. I
- [55] C. Guépin, F. Sarazin, J. Krizmanic, J. Loerincs, A. Olinto, and A. Piccone, “Geometrical Constraints of Observing Very High Energy Earth-Skimming Neutrinos from Space,” *JCAP* **1903** no. 03, (2019) 021, [arXiv:1812.07596 \[astro-ph.IM\]](#). I, 1
- [56] M. H. Reno, J. F. Krizmanic, and T. M. Venters, “Cosmic tau neutrino detection via Cherenkov signals from air showers from Earth-emerging taus,” [arXiv:1902.11287 \[astro-ph.HE\]](#). I, II, II, IV, A, A
- [57] K. Kovarik *et al.*, “nCTEQ15 - Global analysis of nuclear parton distributions with uncertainties in the CTEQ framework,” *Phys. Rev.* **D93** no. 8, (2016) 085037, [arXiv:1509.00792 \[hep-ph\]](#). II
- [58] H. Abramowicz, E. M. Levin, A. Levy, and U. Maor, “A Parametrization of sigma-T (gamma* p) above the resonance region $Q^{*2} \lesssim 0$,” *Phys. Lett.* **B269** (1991) 465–476. II
- [59] H. Abramowicz and A. Levy, “The ALLM parameterization of $\sigma(\text{tot})(\gamma^* p)$: An Update,” [arXiv:hep-ph/9712415 \[hep-ph\]](#). II
- [60] G. J. Feldman and R. D. Cousins, “A Unified approach to the classical statistical analysis of small signals,” *Phys. Rev.* **D57** (1998) 3873–3889, [arXiv:physics/9711021 \[physics.data-an\]](#). II
- [61] **ANTARES**, **IceCube**, **Pierre Auger**, **LIGO Scientific**, **Virgo** Collaboration, A. Albert *et al.*, “Search for High-energy Neutrinos from Binary Neutron Star Merger GW170817 with ANTARES, IceCube, and the Pierre Auger Observatory,” *Astrophys. J.* **850** no. 2, (2017) L35, [arXiv:1710.05839 \[astro-ph.HE\]](#). II, 2, 4, IIIB1, IIIB2, IV
- [62] L. A. Anchordoqui, J. L. Feng, H. Goldberg, and A. D. Shapere, “Neutrino bounds on astrophysical sources and new physics,” *Phys. Rev.* **D66** (2002) 103002, [arXiv:hep-ph/0207139 \[hep-ph\]](#). 2
- [63] **Telescope Array** Collaboration, R. U. Abbasi *et al.*, “Indications of Intermediate-Scale Anisotropy of Cosmic Rays with Energy Greater Than 57 EeV in the Northern Sky Measured with the Surface Detector of the Telescope Array Experiment,” *Astrophys. J.* **790** (2014) L21, [arXiv:1404.5890 \[astro-ph.HE\]](#). 3
- [64] **Telescope Array** Collaboration, R. U. Abbasi, Lundquist, P. Sokolsky, and P. Tinyakov, “Evidence of Intermediate-Scale Energy Spectrum Anisotropy in the Northern Hemisphere from Telescope Array,” *PoS ICRC2017* (2018) 513. 3
- [65] **Pierre Auger** Collaboration, A. Aab *et al.*, “An Indication of anisotropy in arrival directions of ultra-high-energy cosmic rays through comparison to the flux pattern of extragalactic gamma-ray sources,” *Astrophys. J.* **853** no. 2, (2018) L29, [arXiv:1801.06160 \[astro-ph.HE\]](#). 3
- [66] **Telescope Array** Collaboration, R. U. Abbasi *et al.*, “Testing a Reported Correlation between Arrival Directions of Ultra-high-energy Cosmic Rays and a Flux Pattern from nearby Starburst Galaxies using Telescope Array Data,” *Astrophys. J.* **867** no. 2, (2018) L27, [arXiv:1809.01573 \[astro-ph.HE\]](#).
- [67] L. A. Anchordoqui, “Ultra-High-Energy Cosmic Rays,” *Phys. Rep.* **801** (2019) 1–93, [arXiv:1807.09645 \[astro-ph.HE\]](#). 3
- [68] **IceCube** Collaboration, M. G. Aartsen *et al.*, “Neutrino emission from the direction of the blazar TXS 0506+056 prior to the

- IceCube-170922A alert,” *Science* **361** no. 6398, (2018) 147–151, [arXiv:1807.08794](#) [[astro-ph.HE](#)]. 3, III B 1
- [69] J. P. Huchra *et al.*, “The 2MASS Redshift Survey—Description and Data Release,” *ApJS* **199** (Apr., 2012) 26, [arXiv:1108.0669](#). III A
- [70] M. F. Skrutskie *et al.*, “The Two Micron All Sky Survey (2MASS),” *AJ* **131** (Feb., 2006) 1163–1183. III A
- [71] D. J. Fixsen, E. S. Cheng, J. M. Gales, J. C. Mather, R. A. Shafer, and E. L. Wright, “The Cosmic Microwave Background spectrum from the full COBE FIRAS data set,” *Astrophys. J.* **473** (1996) 576, [arXiv:astro-ph/9605054](#) [[astro-ph](#)]. III A
- [72] T. M. Davis and M. I. Scrimgeour, “Deriving accurate peculiar velocities (even at high redshift),” *Mon. Not. Roy. Astron. Soc.* **442** no. 2, (2014) 1117–1122, [arXiv:1405.0105](#) [[astro-ph.CO](#)]. III A
- [73] D. W. Hogg, “Distance measures in cosmology,” [arXiv:astro-ph/9905116](#) [[astro-ph](#)]. B
- [74] P. J. E. Peebles, *Principles of Physical Cosmology*. 1993. III A
- [75] **Planck** Collaboration, N. Aghanim *et al.*, “Planck 2018 results. VI. Cosmological parameters,” [arXiv:1807.06209](#) [[astro-ph.CO](#)]. 1
- [76] A. G. Riess, L. Macri, S. Casertano, H. Lampeitl, H. C. Ferguson, A. V. Filippenko, S. W. Jha, W. Li, and R. Chornock, “A 3% Solution: Determination of the Hubble Constant with the Hubble Space Telescope and Wide Field Camera 3,” *Astrophys. J.* **730** (2011) 119, [arXiv:1103.2976](#) [[astro-ph.CO](#)]. [Erratum: *Astrophys. J.* 732, 129 (2011)]. 1
- [77] S. H. Lim, H. J. Mo, Y. Lu, H. Wang, and X. Yang, “Galaxy groups in the low-redshift Universe,” *MNRAS* **470** no. 3, (Sep, 2017) 2982–3005, [arXiv:1706.02307](#) [[astro-ph.GA](#)]. III A, III A, III A
- [78] R. B. Tully, L. Rizzi, E. J. Shaya, H. M. Courtois, D. I. Makarov, and B. A. Jacobs, “The Extragalactic Distance Database,” *arXiv e-prints* (Feb, 2009) [arXiv:0902.3668](#), [arXiv:0902.3668](#) [[astro-ph.CO](#)]. III A
- [79] M. Cohen, W. A. Wheaton, and S. T. Megeath, “Spectral irradiance calibration in the infrared. 14: The Absolute calibration of 2MASS,” *Astron. J.* **126** (2003) 1090, [arXiv:astro-ph/0304350](#) [[astro-ph](#)]. III A
- [80] **SDSS** Collaboration, M. Bernardi *et al.*, “Early -type galaxies in the SDSS. I. The Sample,” *Astron. J.* **125** (2003) 1817, [arXiv:astro-ph/0301631](#) [[astro-ph](#)]. III A
- [81] E. F. Bell, D. H. McIntosh, N. Katz, and M. D. Weinberg, “The optical and near-infrared properties of galaxies. 1. Luminosity and stellar mass functions,” *Astrophys. J. Suppl.* **149** (2003) 289, [arXiv:astro-ph/0302543](#) [[astro-ph](#)]. III A
- [82] J. A. Peacock, *Cosmological Physics*. Jan., 1999. III A
- [83] R. Blandford, D. Meier, and A. Readhead, “Relativistic Jets in Active Galactic Nuclei,” [arXiv:1812.06025](#) [[astro-ph.HE](#)]. III B 1
- [84] A. M. Hillas, “The Origin of Ultra-High-Energy Cosmic Rays,” *Ann. Rev. Astron. & Astrophys.* **22** (Jan, 1984) 425–444. III B 1
- [85] K. Kotera and A. V. Olinto, “The Astrophysics of Ultrahigh-Energy Cosmic Rays,” *Ann. Rev. Astron. & Astrophys.* **49** no. 1, (Sep, 2011) 119–153, [arXiv:1101.4256](#) [[astro-ph.HE](#)]. III B 1
- [86] P. L. Biermann and P. A. Strittmatter, “Synchrotron emission from shock waves in active galactic nuclei,” *Astrophys. J.* **322** (1987) 643–649. III B 1
- [87] R. J. Protheroe and A. P. Szabo, “High energy cosmic rays from active galactic nuclei,” *Phys. Rev. Lett.* **69** no. 20, (Nov, 1992) 2885–2888. III B 1
- [88] J. P. Rachen and P. L. Biermann, “Extragalactic ultrahigh-energy cosmic rays. 1. Contribution from hot spots in FR-II radio galaxies,” *Astron. Astrophys.* **272** (1993) 161–175, [arXiv:astro-ph/9301010](#) [[astro-ph](#)]. III B 1
- [89] G. E. Romero, J. A. Combi, L. A. Anchordoqui, and S. Perez Bergliaffa, “A possible source of extragalactic cosmic rays with arrival energies beyond the GZK cutoff,” *Astropart. Phys.* **5** (1996) 279–283, [arXiv:gr-qc/9511031](#) [[gr-qc](#)].
- [90] **Pierre Auger** Collaboration, P. Abreu *et al.*, “Update on the correlation of the highest energy cosmic rays with nearby extragalactic matter,” *Astroparticle Physics* **34** no. 5, (Jan, 2010) 314–326, [arXiv:1009.1855](#) [[astro-ph.HE](#)].
- [91] S. Wykes *et al.*, “Mass entrainment and turbulence-driven acceleration of ultra-high energy cosmic rays in Centaurus A,” *Astron. Astrophys.* **558** (2013) A19, [arXiv:1305.2761](#) [[astro-ph.HE](#)].
- [92] J. H. Matthews, A. R. Bell, K. M. Blundell, and A. T. Araudo, “Fornax A, Centaurus A, and other radio galaxies as sources of ultrahigh energy cosmic rays,” *Mon. Not. Roy. Astron. Soc.* **479** no. 1, (2018) L76–L80, [arXiv:1805.01902](#) [[astro-ph.HE](#)]. III B 1
- [93] F. W. Stecker, C. Done, M. H. Salamon, and P. Sommers, “High-energy neutrinos from active galactic nuclei,” *Phys. Rev. Lett.* **66** no. 21, (May, 1991) 2697–2700. III B 1, III B 1
- [94] A. P. Szabo and R. J. Protheroe, “Implications of particle acceleration in active galactic nuclei for cosmic rays and high energy neutrino astronomy,” *Astroparticle Physics* **2** no. 4, (Oct, 1994) 375–392, [arXiv:astro-ph/9405020](#) [[astro-ph](#)]. III B 1
- [95] S. H. Margolis, D. N. Schramm, and R. Silberberg, “Ultrahigh-energy neutrino astronomy,” *ApJ* **221** (May, 1978) 990–1002.
- [96] D. Eichler, “High-energy neutrino astronomy: a probe of galactic nuclei?,” *ApJ* **232** (Aug, 1979)

- 106–112.
- [97] K. Mannheim and P. L. Biermann, “Photomeson production in active galactic nuclei,” *Astron. & Astrophys.* **221** (Sep, 1989) 211–220.
 - [98] M. C. Begelman, B. Rudak, and M. Sikora, “Consequences of Relativistic Proton Injection in Active Galactic Nuclei,” *ApJ* **362** (Oct, 1990) 38.
 - [99] A. Atoyan and C. D. Dermer, “High-Energy Neutrinos from Photomeson Processes in Blazars,” *Phys. Rev. Lett.* **87** no. 22, (Nov, 2001) 221102, [arXiv:astro-ph/0108053](#) [astro-ph].
 - [100] A. Mücke, R. J. Protheroe, R. Engel, J. P. Rachen, and T. Stanev, “BL Lac objects in the synchrotron proton blazar model,” *Astroparticle Physics* **18** no. 6, (Mar, 2003) 593–613, [arXiv:astro-ph/0206164](#) [astro-ph].
 - [101] S. Hümmer, M. Rieger, F. Spanier, and W. Winter, “Simplified Models for Photohadronic Interactions in Cosmic Accelerators,” *ApJ* **721** no. 1, (Sep, 2010) 630–652, [arXiv:1002.1310](#) [astro-ph.HE].
 - [102] M. Böttcher, A. Reimer, K. Sweeney, and A. Prakash, “Leptonic and Hadronic Modeling of Fermi-detected Blazars,” *ApJ* **768** no. 1, (May, 2013) 54, [arXiv:1304.0605](#) [astro-ph.HE].
 - [103] F. Halzen, “Pionic photons and neutrinos from cosmic ray accelerators,” *Astroparticle Physics* **43** (Mar, 2013) 155–162.
 - [104] S. Dimitrakoudis, M. Petropoulou, and A. Mastichiadis, “Self-consistent neutrino and UHE cosmic ray spectra from Mrk 421,” *Astroparticle Physics* **54** (Feb, 2014) 61–66, [arXiv:1310.7923](#) [astro-ph.HE].
 - [105] K. Murase, Y. Inoue, and C. D. Dermer, “Diffuse neutrino intensity from the inner jets of active galactic nuclei: Impacts of external photon fields and the blazar sequence,” *Phys. Rev. D* **90** no. 2, (Jul, 2014) 023007, [arXiv:1403.4089](#) [astro-ph.HE].
 - [106] M. Petropoulou, S. Dimitrakoudis, P. Padovani, A. Mastichiadis, and E. Resconi, “Photohadronic origin of γ -ray BL Lac emission: implications for IceCube neutrinos,” *MNRAS* **448** no. 3, (Apr, 2015) 2412–2429, [arXiv:1501.07115](#) [astro-ph.HE].
 - [107] G. Romero, M. Boettcher, S. Markoff, and F. Tavecchio, “Relativistic Jets in Active Galactic Nuclei and Microquasars,” *Space Sci. Rev.* **207** no. 1–4, (2017) 5–61, [arXiv:1611.09507](#) [astro-ph.HE].
 - [108] A. Reimer, M. Boettcher, and S. Buson, “Cascading Constraints from Neutrino Emitting Blazars: The case of TXS 0506+056,” [arXiv:1812.05654](#) [astro-ph.HE].
 - [109] A. Keivani *et al.*, “A Multimessenger Picture of the Flaring Blazar TXS 0506+056: Implications for High-energy Neutrino Emission and Cosmic-Ray Acceleration,” *ApJ* **864** no. 1, (Sep, 2018) 84, [arXiv:1807.04537](#) [astro-ph.HE].
 - [110] S. Gao, A. Fedynitch, W. Winter, and M. Pohl, “Modelling the coincident observation of a high-energy neutrino and a bright blazar flare,” *Nature Astronomy* **3** (Jan, 2019) 88–92, [arXiv:1807.04275](#) [astro-ph.HE].
 - [111] H. Zhang, K. Fang, H. Li, D. Giannios, M. Böttcher, and S. Buson, “Probing the Emission Mechanism and Magnetic Field of Neutrino Blazars with Multiwavelength Polarization Signatures,” *ApJ* **876** no. 2, (May, 2019) 109, [arXiv:1903.01956](#) [astro-ph.HE].
 - [112] M. Cerruti, A. Zech, C. Boisson, G. Emery, S. Inoue, and J. P. Lenain, “Leptohadronic single-zone models for the electromagnetic and neutrino emission of TXS 0506+056,” *MNRAS* **483** no. 1, (Feb, 2019) L12–L16, [arXiv:1807.04335](#) [astro-ph.HE].
 - [113] L. A. Anchordoqui, D. Hooper, S. Sarkar, and A. M. Taylor, “High-energy neutrinos from astrophysical accelerators of cosmic ray nuclei,” *Astropart. Phys.* **29** (2008) 1–13, [arXiv:astro-ph/0703001](#) [astro-ph]. III B 1, III B 2
 - [114] M. Ajello *et al.*, “The Luminosity Function of Fermi-detected Flat-spectrum Radio Quasars,” *ApJ* **751** no. 2, (Jun, 2012) 108, [arXiv:1110.3787](#) [astro-ph.CO]. III B 1
 - [115] F. W. Stecker and M. H. Salamon, “The Gamma-Ray Background from Blazars: A New Look,” *ApJ* **464** (Jun, 1996) 600, [arXiv:astro-ph/9601120](#) [astro-ph]. III B 1
 - [116] E. Valtaoja, A. Lähteenmäki, H. Teräsranta, and M. Lainela, “Total Flux Density Variations in Extragalactic Radio Sources. I. Decomposition of Variations into Exponential Flares,” *ApJS* **120** no. 1, (Jan, 1999) 95–99.
 - [117] M. L. Lister, “Relativistic Beaming and Flux Variability in Active Galactic Nuclei,” *ApJ* **561** no. 2, (Nov, 2001) 676–683, [arXiv:astro-ph/0107532](#) [astro-ph].
 - [118] I. Liodakis, V. Pavlidou, T. Hovatta, W. Max-Moerbeck, T. J. Pearson, J. L. Richards, and A. C. S. Readhead, “Bimodal radio variability in OVRO-40 m-monitored blazars,” *MNRAS* **467** no. 4, (Jun, 2017) 4565–4576, [arXiv:1702.05493](#) [astro-ph.HE]. III B 1, III B 1
 - [119] J. G. Hills, “Possible power source of Seyfert galaxies and QSOs,” *Nature* **254** no. 5498, (Mar, 1975) 295–298. III B 1
 - [120] M. J. Rees, “Tidal disruption of stars by black holes of 10^6 – 10^8 solar masses in nearby galaxies,” *Nature* **333** no. 6173, (Jun, 1988) 523–528. III B 1, III B 1
 - [121] S. Komossa, “Tidal disruption of stars by supermassive black holes: Status of observations,” *Journal of High Energy Astrophysics* **7** (Sep, 2015) 148–157, [arXiv:1505.01093](#) [astro-ph.HE]. III B 1
 - [122] K. Auchettl, J. Guillochon, and E. Ramirez-Ruiz, “New Physical Insights about Tidal Disruption Events from a Comprehensive Observational Inventory at X-Ray Wavelengths,” *ApJ* **838** no. 2, (Apr, 2017) 149, [arXiv:1611.02291](#)

- [astro-ph.HE]. III B 1
- [123] J. H. Lacy, C. H. Townes, and D. J. Hollenbach, “The nature of the central parsec of the Galaxy,” *ApJ* **262** (Nov, 1982) 120–134. III B 1
- [124] A. Ulmer, “Flares from the Tidal Disruption of Stars by Massive Black Holes,” *ApJ* **514** no. 1, (Mar, 1999) 180–187. III B 1
- [125] C. R. Evans and C. S. Kochanek, “The tidal disruption of a star by a massive black hole,” *ApJL* **346** (Nov., 1989) L13–L16. III B 1
- [126] J. K. Cannizzo, H. M. Lee, and J. Goodman, “The disk accretion of a tidally disrupted star onto a massive black hole,” *ApJ* **351** (Mar., 1990) 38–46. III B 1
- [127] J. R. Cummings *et al.*, “GRB 110328A: Swift detection of a burst,” *GRB Coordinates Network* **11823** (Mar, 2011) 1. III B 1
- [128] J. S. Bloom *et al.*, “A Possible Relativistic Jetted Outburst from a Massive Black Hole Fed by a Tidally Disrupted Star,” *Science* **333** no. 6039, (Jul, 2011) 203, [arXiv:1104.3257](#) [astro-ph.HE]. III B 1
- [129] D. N. Burrows *et al.*, “Relativistic jet activity from the tidal disruption of a star by a massive black hole,” *Nature* **476** no. 7361, (Aug, 2011) 421–424, [arXiv:1104.4787](#) [astro-ph.HE].
- [130] B. A. Zauderer *et al.*, “Birth of a relativistic outflow in the unusual γ -ray transient Swift J164449.3+573451,” *Nature* **476** no. 7361, (Aug, 2011) 425–428, [arXiv:1106.3568](#) [astro-ph.HE]. III B 1
- [131] G. R. Farrar and A. Gruzinov, “Giant AGN Flares and Cosmic Ray Bursts,” *Astrophys. J.* **693** (2009) 329–332, [arXiv:0802.1074](#) [astro-ph]. III B 1
- [132] G. R. Farrar and T. Piran, “Tidal disruption jets as the source of Ultra-High Energy Cosmic Rays,” *arXiv e-prints* (Nov, 2014) [arXiv:1411.0704](#), [arXiv:1411.0704](#) [astro-ph.HE].
- [133] D. N. Pfeffer, E. D. Kovetz, and M. Kamionkowski, “Ultrahigh-energy cosmic ray hotspots from tidal disruption events,” *MNRAS* **466** no. 3, (Apr, 2017) 2922–2926, [arXiv:1512.04959](#) [astro-ph.HE]. III B 1
- [134] X.-Y. Wang, R.-Y. Liu, Z.-G. Dai, and K. S. Cheng, “Probing the tidal disruption flares of massive black holes with high-energy neutrinos,” *Phys. Rev. D* **84** no. 8, (Oct, 2011) 081301, [arXiv:1106.2426](#) [astro-ph.HE]. III B 1, III B 1
- [135] X.-Y. Wang and R.-Y. Liu, “Tidal disruption jets of supermassive black holes as hidden sources of cosmic rays: Explaining the IceCube TeV–PeV neutrinos,” *Phys. Rev. D* **93** no. 8, (Apr, 2016) 083005, [arXiv:1512.08596](#) [astro-ph.HE]. III B 1
- [136] N. Senno, K. Murase, and P. Meszaros, “High-energy Neutrino Flares from X-Ray Bright and Dark Tidal Disruption Events,” *Astrophys. J.* **838** no. 1, (2017) 3, [arXiv:1612.00918](#) [astro-ph.HE].
- [137] D. Biehl, D. Boncioli, C. Lunardini, and W. Winter, “Tidally disrupted stars as a possible origin of both cosmic rays and neutrinos at the highest energies,” *Sci. Rep.* **8** no. 1, (2018) 10828, [arXiv:1711.03555](#) [astro-ph.HE]. III B 1
- [138] D. Guetta, D. Hooper, J. Alvarez-Muniz, F. Halzen, and E. Reuveni, “Neutrinos from individual gamma-ray bursts in the BATSE catalog,” *Astropart. Phys.* **20** (2004) 429–455, [arXiv:astro-ph/0302524](#) [astro-ph]. III B 1, III B 2
- [139] A. Boehle *et al.*, “An Improved Distance and Mass Estimate for Sgr A* from a Multistar Orbit Analysis,” *ApJ* **830** no. 1, (Oct, 2016) 17, [arXiv:1607.05726](#) [astro-ph.GA]. III B 1
- [140] J. E. Gunn and J. P. Ostriker, “Acceleration of high-energy cosmic rays by pulsars,” *Phys. Rev. Lett.* **22** (1969) 728–731. III B 1
- [141] A. R. Bell, “Cosmic ray acceleration in pulsar-driven supernova remnants,” *MNRAS* **257** (Aug, 1992) 493–500.
- [142] P. Blasi, R. I. Epstein, and A. V. Olinto, “Ultrahigh-energy cosmic rays from young neutron star winds,” *Astrophys. J.* **533** (2000) L123, [arXiv:astro-ph/9912240](#) [astro-ph]. III B 1
- [143] J. Arons, “Magnetars in the Metagalaxy: An Origin for Ultra-High-Energy Cosmic Rays in the Nearby Universe,” *ApJ* **589** no. 2, (Jun, 2003) 871–892, [arXiv:astro-ph/0208444](#) [astro-ph].
- [144] K. Fang, K. Kotera, and A. V. Olinto, “Newly Born Pulsars as Sources of Ultrahigh Energy Cosmic Rays,” *ApJ* **750** no. 2, (May, 2012) 118, [arXiv:1201.5197](#) [astro-ph.HE]. III B 1, III B 1
- [145] V. M. Kaspi and A. Beloborodov, “Magnetars,” *Ann. Rev. Astron. Astrophys.* **55** (2017) 261–301, [arXiv:1703.00068](#) [astro-ph.HE]. III B 1, III B 1
- [146] B. D. Metzger and A. L. Piro, “Optical and X-ray emission from stable millisecond magnetars formed from the merger of binary neutron stars,” *MNRAS* **439** no. 4, (Apr, 2014) 3916–3930, [arXiv:1311.1519](#) [astro-ph.HE]. III B 1, III B 2
- [147] **LIGO Scientific, Virgo, Fermi-GBM, INTEGRAL Collaboration**, B. P. Abbott *et al.*, “Gravitational Waves and Gamma-rays from a Binary Neutron Star Merger: GW170817 and GRB 170817A,” *Astrophys. J.* **848** no. 2, (2017) L13, [arXiv:1710.05834](#) [astro-ph.HE]. III B 1
- [148] **LIGO Scientific, VIRGO Collaboration**, J. Aasi *et al.*, “Characterization of the LIGO detectors during their sixth science run,” *Class. Quant. Grav.* **32** no. 11, (2015) 115012, [arXiv:1410.7764](#) [gr-qc]. III B 1
- [149] **VIRGO Collaboration**, F. Acernese *et al.*, “Advanced Virgo: a second-generation interferometric gravitational wave detector,” *Class. Quant. Grav.* **32** no. 2, (2015) 024001, [arXiv:1408.3978](#) [gr-qc]. III B 1
- [150] **LIGO Scientific, Virgo Collaboration**, B. P. Abbott *et al.*, “GWTC-1: A Gravitational-Wave Transient Catalog of Compact Binary Mergers Observed by LIGO and Virgo during the First

- and Second Observing Runs,” [arXiv:1811.12907 \[astro-ph.HE\]](#). III B 1, III B 1
- [151] R. D. Blandford and R. L. Znajek, “Electromagnetic extractions of energy from Kerr black holes,” *Mon. Not. Roy. Astron. Soc.* **179** (1977) 433–456. III B 1
- [152] R. Perna, D. Lazzati, and W. Farr, “Limits on electromagnetic counterparts of gravitational wave-detected binary black hole mergers,” *Astrophys. J.* **875** no. 1, (2019) 49, [arXiv:1901.04522 \[astro-ph.HE\]](#). III B 1
- [153] V. Connaughton *et al.*, “Fermi GBM Observations of LIGO Gravitational Wave event GW150914,” *Astrophys. J.* **826** no. 1, (2016) L6, [arXiv:1602.03920 \[astro-ph.HE\]](#). III B 1
- [154] A. Loeb, “Electromagnetic Counterparts to Black Hole Mergers Detected by LIGO,” *Astrophys. J.* **819** no. 2, (2016) L21, [arXiv:1602.04735 \[astro-ph.HE\]](#). III B 1
- [155] R. Perna, D. Lazzati, and B. Giacomazzo, “Short Gamma-Ray Bursts from the Merger of Two Black Holes,” *Astrophys. J.* **821** no. 1, (2016) L18, [arXiv:1602.05140 \[astro-ph.HE\]](#). III B 1
- [156] K. Murase, K. Kashiyama, P. Mészáros, I. Shoemaker, and N. Senno, “Ultrafast Outflows from Black Hole Mergers with a Minidisk,” *Astrophys. J.* **822** no. 1, (2016) L9, [arXiv:1602.06938 \[astro-ph.HE\]](#).
- [157] S. E. Woosley, “The Progenitor of Gw150914,” *Astrophys. J.* **824** no. 1, (2016) L10, [arXiv:1603.00511 \[astro-ph.HE\]](#).
- [158] A. Janiuk, M. Bejger, S. Charzyński, and P. Sukova, “On the possible gamma-ray burst–gravitational wave association in GW150914,” *New Astron.* **51** (2017) 7–14, [arXiv:1604.07132 \[astro-ph.HE\]](#).
- [159] I. Bartos, B. Kocsis, Z. Haiman, and S. Márka, “Rapid and Bright Stellar-mass Binary Black Hole Mergers in Active Galactic Nuclei,” *Astrophys. J.* **835** no. 2, (2017) 165, [arXiv:1602.03831 \[astro-ph.HE\]](#).
- [160] S. E. d. Mink and A. King, “Electromagnetic signals following stellar-mass black hole mergers,” *Astrophys. J.* **839** no. 1, (2017) L7, [arXiv:1703.07794 \[astro-ph.HE\]](#).
- [161] A. Khan, V. Paschalidis, M. Ruiz, and S. L. Shapiro, “Disks Around Merging Binary Black Holes: From GW150914 to Supermassive Black Holes,” *Phys. Rev.* **D97** no. 4, (2018) 044036, [arXiv:1801.02624 \[astro-ph.HE\]](#).
- [162] R. G. Martin, C. Nixon, F.-G. Xie, and A. King, “Circumbinary discs around merging stellar-mass black holes,” *Mon. Not. Roy. Astron. Soc.* **480** no. 4, (2018) 4732–4737, [arXiv:1808.06023 \[astro-ph.HE\]](#). III B 1
- [163] S. L. Liebling and C. Palenzuela, “Electromagnetic Luminosity of the Coalescence of Charged Black Hole Binaries,” *Phys. Rev.* **D94** no. 6, (2016) 064046, [arXiv:1607.02140 \[gr-qc\]](#). III B 1
- [164] B. Zhang, “Mergers of Charged Black Holes: Gravitational Wave Events, Short Gamma-Ray Bursts, and Fast Radio Bursts,” *Astrophys. J.* **827** no. 2, (2016) L31, [arXiv:1602.04542 \[astro-ph.HE\]](#).
- [165] T. Liu, G. E. Romero, M.-L. Liu, and A. Li, “Fast Radio Bursts and Their Gamma-ray or Radio Afterglows as Kerr–newman Black Hole Binaries,” *Astrophys. J.* **826** no. 1, (2016) 82, [arXiv:1602.06907 \[astro-ph.HE\]](#).
- [166] F. Fraschetti, “Possible role of magnetic reconnection in the electromagnetic counterpart of binary black hole merger,” *JCAP* **1804** no. 04, (2018) 054, [arXiv:1603.01950 \[astro-ph.HE\]](#). III B 1
- [167] L. A. Anchordoqui, “Neutrino lighthouse powered by Sagittarius A* disk dynamo,” *Phys. Rev.* **D94** (2016) 023010, [arXiv:1606.01816 \[astro-ph.HE\]](#). III B 1
- [168] C. Guépin and K. Kotera, “Can we observe neutrino flares in coincidence with explosive transients?,” *Astron. Astrophys.* **603** (2017) A76, [arXiv:1701.07038 \[astro-ph.HE\]](#). III B 1
- [169] K. Ohsuga, M. Mori, T. Nakamoto, and S. Mineshige, “Supercritical Accretion Flows around Black Holes: Two-dimensional, Radiation Pressure-dominated Disks with Photon Trapping,” *ApJ* **628** no. 1, (Jul, 2005) 368–381, [arXiv:astro-ph/0504168 \[astro-ph\]](#). III B 2
- [170] M. C. Miller, “Disk Winds as an Explanation for Slowly Evolving Temperatures in Tidal Disruption Events,” *ApJ* **805** no. 1, (May, 2015) 83, [arXiv:1502.03284 \[astro-ph.GA\]](#).
- [171] J. C. McKinney, L. Dai, and M. J. Avara, “Efficiency of super-Eddington magnetically-arrested accretion,” *MNRAS* **454** no. 1, (Nov, 2015) L6–L10, [arXiv:1508.02433 \[astro-ph.HE\]](#). III B 2
- [172] S. S. Kim, M.-G. Park, and H. M. Lee, “The Stream-Stream Collision after the Tidal Disruption of a Star around a Massive Black Hole,” *ApJ* **519** no. 2, (Jul, 1999) 647–657, [arXiv:astro-ph/9902132 \[astro-ph\]](#). III B 2
- [173] Y.-F. Jiang, J. Guillochon, and A. Loeb, “Prompt Radiation and Mass Outflows from the Stream-Stream Collisions of Tidal Disruption Events,” *ApJ* **830** no. 2, (Oct, 2016) 125, [arXiv:1603.07733 \[astro-ph.HE\]](#). III B 2
- [174] I. Tamborra, S. Ando, and K. Murase, “Star-forming galaxies as the origin of diffuse high-energy backgrounds: Gamma-ray and neutrino connections, and implications for starburst history,” *JCAP* **1409** (2014) 043, [arXiv:1404.1189 \[astro-ph.HE\]](#). III B 2
- [175] IceCube Collaboration, M. G. Aartsen *et al.*, “The IceCube Neutrino Observatory - Contributions to ICRC 2017 Part II: Properties of the Atmospheric and Astrophysical Neutrino Flux,” [arXiv:1710.01191 \[astro-ph.HE\]](#). III B 2
- [176] J. L. Donley, W. N. Brandt, M. C. Eracleous, and T. Boller, “Large-amplitude x-ray outbursts from galactic nuclei: A Systematic survey using

- ROSAT archival data,” *Astron. J.* **124** (2002) 1308, [arXiv:astro-ph/0206291 \[astro-ph\]](#). 4
- [177] J. Magorrian and S. Tremaine, “Rates of tidal disruption of stars by massive central black holes,” *Mon. Not. Roy. Astron. Soc.* **309** (1999) 447, [arXiv:astro-ph/9902032 \[astro-ph\]](#). III B 2
- [178] B. Paczynski, “Gamma-ray bursters at cosmological distances,” *ApJL* **308** (Sept., 1986) L43–L46. III B 2
- [179] J. Goodman, “Are gamma-ray bursts optically thick?,” *ApJL* **308** (Sept., 1986) L47–L50.
- [180] A. Shemi and T. Piran, “The appearance of cosmic fireballs,” *ApJL* **365** (Dec., 1990) L55–L58.
- [181] P. Meszaros and M. J. Rees, “Relativistic fireballs and their impact on external matter - Models for cosmological gamma-ray bursts,” *ApJ* **405** (Mar., 1993) 278–284. III B 2
- [182] E. Waxman, “Cosmological gamma-ray bursts and the highest energy cosmic rays,” *Phys. Rev. Lett.* **75** (1995) 386–389, [arXiv:astro-ph/9505082 \[astro-ph\]](#). III B 2
- [183] K. Murase and S. Nagataki, “High Energy Neutrino Flash from Far-UV/X-ray Flares of Gamma-Ray Bursts,” *Phys. Rev. Lett.* **97** (2006) 051101, [arXiv:astro-ph/0604437 \[astro-ph\]](#). III B 2
- [184] S. Hummer, P. Baerwald, and W. Winter, “Neutrino Emission from Gamma-Ray Burst Fireballs, Revised,” *Phys. Rev. Lett.* **108** (2012) 231101, [arXiv:1112.1076 \[astro-ph.HE\]](#).
- [185] P. Baerwald, M. Bustamante, and W. Winter, “UHECR escape mechanisms for protons and neutrons from GRBs, and the cosmic ray-neutrino connection,” *Astrophys. J.* **768** (2013) 186, [arXiv:1301.6163 \[astro-ph.HE\]](#).
- [186] M. Bustamante, P. Baerwald, K. Murase, and W. Winter, “Neutrino and cosmic-ray emission from multiple internal shocks in gamma-ray bursts,” [arXiv:1409.2874 \[astro-ph.HE\]](#). [Nature Commun.6,6783(2015)].
- [187] M. Vietri, “On the acceleration of ultrahigh-energy cosmic rays in gamma-ray bursts,” *Astrophys. J.* **453** (1995) 883–889, [arXiv:astro-ph/9506081 \[astro-ph\]](#).
- [188] C. D. Dermer and A. Atoyan, “Ultrahigh energy cosmic rays, cascade gamma-rays, and high-energy neutrinos from gamma-ray bursts,” *New J. Phys.* **8** (2006) 122, [arXiv:astro-ph/0606629 \[astro-ph\]](#).
- [189] X.-Y. Wang, S. Razzaque, and P. Meszaros, “On the Origin and Survival of UHE Cosmic-Ray Nuclei in GRBs and Hypernovae,” *Astrophys. J.* **677** (2008) 432–440, [arXiv:0711.2065 \[astro-ph\]](#).
- [190] K. Murase, K. Ioka, S. Nagataki, and T. Nakamura, “High-energy cosmic-ray nuclei from high- and low-luminosity gamma-ray bursts and implications for multi-messenger astronomy,” *Phys. Rev. D* **78** (2008) 023005, [arXiv:0801.2861 \[astro-ph\]](#).
- [191] N. Globus, D. Allard, R. Mochkovitch, and E. Parizot, “UHECR acceleration at GRB internal shocks,” *Mon. Not. Roy. Astron. Soc.* **451** no. 1, (2015) 751–790, [arXiv:1409.1271 \[astro-ph.HE\]](#).
- [192] B. T. Zhang, K. Murase, S. S. Kimura, S. Horiuchi, and P. Mészáros, “Low-luminosity gamma-ray bursts as the sources of ultrahigh-energy cosmic ray nuclei,” *Phys. Rev. D* **97** no. 8, (2018) 083010, [arXiv:1712.09984 \[astro-ph.HE\]](#). III B 2
- [193] P. Mészáros, “Ultra-high Energy Cosmic Rays and Neutrinos from Gamma-Ray Bursts, Hypernovae and Galactic Shocks,” *Nucl. Phys. Proc. Suppl.* **256–257** (2014) 241–251, [arXiv:1407.5671 \[astro-ph.HE\]](#). III B 2
- [194] T. Sakamoto, S. D. Barthelmy, W. H. Baumgartner, J. R. Cummings, E. E. Fenimore, N. Gehrels, H. A. Krimm, C. B. Markwardt, D. M. Palmer, and A. M. Parsons, “The Second Swift Burst Alert Telescope Gamma-Ray Burst Catalog,” *ApJS* **195** no. 1, (Jul, 2011) 2, [arXiv:1104.4689 \[astro-ph.HE\]](#). III B 2
- [195] D. Wanderman and T. Piran, “The rate, luminosity function and time delay of non-Collapsar short GRBs,” *Mon. Not. Roy. Astron. Soc.* **448** no. 4, (2015) 3026–3037, [arXiv:1405.5878 \[astro-ph.HE\]](#). III B 2
- [196] A. Lien, T. Sakamoto, N. Gehrels, D. M. Palmer, S. D. Barthelmy, C. Graziani, and J. K. Cannizzo, “Probing the Cosmic Gamma-Ray Burst Rate with Trigger Simulations of the Swift Burst Alert Telescope,” *Astrophys. J.* **783** no. 1, (2014) 24, [arXiv:1311.4567 \[astro-ph.HE\]](#). III B 2
- [197] K. Murase, P. Meszaros, and B. Zhang, “Probing the birth of fast rotating magnetars through high-energy neutrinos,” *Phys. Rev. D* **79** (2009) 103001, [arXiv:0904.2509 \[astro-ph.HE\]](#). III B 2
- [198] K. Fang, K. Kotera, K. Murase, and A. V. Olinto, “Testing the Newborn Pulsar Origin of Ultrahigh Energy Cosmic Rays with EeV Neutrinos,” *Phys. Rev. D* **90** no. 10, (2014) 103005, [arXiv:1311.2044 \[astro-ph.HE\]](#). [Phys. Rev.D90,103005(2014)]. III B 2
- [199] R. M. Quimby, F. Yuan, C. Akerlof, and J. C. Wheeler, “Rates of Superluminous Supernovae at $z > 0.2$,” *Mon. Not. Roy. Astron. Soc.* **431** (2013) 912, [arXiv:1302.0911 \[astro-ph.CO\]](#). III B 2
- [200] V. A. Villar, M. Nicholl, and E. Berger, “Superluminous Supernovae in LSST: Rates, Detection Metrics, and Light Curve Modeling,” *Astrophys. J.* **869** no. 2, (2018) 166, [arXiv:1809.07343 \[astro-ph.HE\]](#). III B 2
- [201] M. Taylor *et al.*, “The Core Collapse Supernova Rate from the SDSS-II Supernova Survey,” *Astrophys. J.* **792** (2014) 135, [arXiv:1407.0999 \[astro-ph.SR\]](#). III B 2
- [202] A. L. Piro and J. A. Kollmeier, “Ultrahigh-energy Cosmic Rays From the ‘en Caul’ Birth of Magnetars,” *Astrophys. J.* **826** no. 1, (2016) 97,

- [arXiv:1601.02625 \[astro-ph.HE\]](#). III B 2, III B 2, III B 2
- [203] S. Ji, R. T. Fisher, E. García-Berro, P. Tzeferacos, G. Jordan, D. Lee, P. Lorén-Aguilar, P. Cremer, and J. Behrends, “The Post-Merger Magnetized Evolution of White Dwarf Binaries: The Double-Degenerate Channel of Sub-Chandrasekhar Type Ia Supernovae and the Formation of Magnetized White Dwarfs,” *Astrophys. J.* **773** (2013) 136, [arXiv:1302.5700 \[astro-ph.SR\]](#). III B 2
- [204] A. M. Beloborodov, “Magnetically powered outbursts from white dwarf mergers,” *Mon. Not. Roy. Astron. Soc.* **438** no. 1, (2014) 169–176, [arXiv:1311.0668 \[astro-ph.HE\]](#).
- [205] C. Zhu, R. Pakmor, M. H. van Kerkwijk, and P. Chang, “Magnetized Moving Mesh Merger of a Carbon-Oxygen White Dwarf Binary,” *ApJ* **806** no. 1, (Jun, 2015) L1, [arXiv:1504.01732 \[astro-ph.SR\]](#). III B 2
- [206] C. Badenes and D. Maoz, “The Merger Rate of Binary White Dwarfs in the Galactic Disk,” *ApJ* **749** no. 1, (Apr, 2012) L11, [arXiv:1202.5472 \[astro-ph.SR\]](#). III B 2
- [207] ANITA Collaboration, P. W. Gorham *et al.*, “Characteristics of Four Upward-pointing Cosmic-ray-like Events Observed with ANITA,” *Phys. Rev. Lett.* **117** no. 7, (2016) 071101, [arXiv:1603.05218 \[astro-ph.HE\]](#). IV
- [208] ANITA Collaboration, P. W. Gorham *et al.*, “Observation of an Unusual Upward-going Cosmic-ray-like Event in the Third Flight of ANITA,” *Phys. Rev. Lett.* **121** no. 16, (2018) 161102, [arXiv:1803.05088 \[astro-ph.HE\]](#). IV
- [209] A. Romero-Wolf *et al.*, “Comprehensive analysis of anomalous ANITA events disfavors a diffuse tau-neutrino flux origin,” *Phys. Rev. D* **99** no. 6, (2019) 063011, [arXiv:1811.07261 \[astro-ph.HE\]](#). IV
- [210] D. B. Fox, S. Sigurdsson, S. Shandera, P. Mészáros, K. Murase, M. Mostafá, and S. Coutu, “The ANITA Anomalous Events as Signatures of a Beyond Standard Model Particle, and Supporting Observations from IceCube,” *Submitted to: Phys. Rev. D* (2018), [arXiv:1809.09615 \[astro-ph.HE\]](#). IV
- [211] J. F. Cherry and I. M. Shoemaker, “Sterile neutrino origin for the upward directed cosmic ray showers detected by ANITA,” *Phys. Rev. D* **99** no. 6, (2019) 063016, [arXiv:1802.01611 \[hep-ph\]](#). IV
- [212] L. A. Anchordoqui, V. Barger, J. G. Learned, D. Marfatia, and T. J. Weiler, “Upgoing ANITA events as evidence of the CPT symmetric universe,” *LHEP* **1** no. 1, (2018) 13–16, [arXiv:1803.11554 \[hep-ph\]](#).
- [213] G.-y. Huang, “Sterile neutrinos as a possible explanation for the upward air shower events at ANITA,” *Phys. Rev. D* **98** no. 4, (2018) 043019, [arXiv:1804.05362 \[hep-ph\]](#).
- [214] J. H. Collins, P. S. Bhupal Dev, and Y. Sui, “R-parity Violating Supersymmetric Explanation of the Anomalous Events at ANITA,” *Phys. Rev. D* **99** no. 4, (2019) 043009, [arXiv:1810.08479 \[hep-ph\]](#).
- [215] B. Chauhan and S. Mohanty, “Leptoquark solution for both the flavor and ANITA anomalies,” *Phys. Rev. D* **99** no. 9, (2019) 095018, [arXiv:1812.00919 \[hep-ph\]](#).
- [216] L. A. Anchordoqui and I. Antoniadis, “Supersymmetric sphaleron configurations as the origin of the perplexing ANITA events,” *Phys. Lett. B* **790** (2019) 578–582, [arXiv:1812.01520 \[hep-ph\]](#).
- [217] L. Heurtier, Y. Mambrini, and M. Pierre, “Dark matter interpretation of the ANITA anomalous events,” *Phys. Rev. D* **99** no. 9, (2019) 095014, [arXiv:1902.04584 \[hep-ph\]](#).
- [218] D. Hooper, S. Wegsman, C. Deaconu, and A. Vieregge, “Superheavy Dark Matter and ANITA’s Anomalous Events,” [arXiv:1904.12865 \[astro-ph.HE\]](#).
- [219] J. M. Cline, C. Gross, and W. Xue, “Can the ANITA anomalous events be due to new physics?,” [arXiv:1904.13396 \[hep-ph\]](#).
- [220] I. Esteban, J. Lopez-Pavon, I. Martinez-Soler, and J. Salvado, “Looking at the axionic dark sector with ANITA,” [arXiv:1905.10372 \[hep-ph\]](#).
- [221] L. Heurtier, D. Kim, J.-C. Park, and S. Shin, “Explaining the ANITA Anomaly with Inelastic Boosted Dark Matter,” [arXiv:1905.13223 \[hep-ph\]](#). IV
- [222] K. D. de Vries and S. Prohira, “Coherent transition radiation from the geomagnetically-induced current in cosmic-ray air showers: Implications for the anomalous events observed by ANITA,” [arXiv:1903.08750 \[astro-ph.HE\]](#). IV
- [223] I. M. Shoemaker, A. Kusenko, P. K. Munneke, A. Romero-Wolf, D. M. Schroeder, and M. J. Siegart, “Reflections On the Anomalous ANITA Events: The Antarctic Subsurface as a Possible Explanation,” [arXiv:1905.02846 \[astro-ph.HE\]](#). IV